Ferrocenyl Iron as a Donor Group for Complexed Silver in Ferrocenyldimethyl[2.2]cryptand: A Redox-Switched Receptor Effective in Water

Julio C. Medina, Timothy T. Goodnow, Maria T. Rojas, Jerry L. Atwood,[‡] Bert C. Lynn,*,# Angel E. Kaifer,*,§ and George W. Gokel*,†

Contribution from the Departments of Chemistry, University of Miami, Coral Gables, Florida 33124, and University of Alabama, Tuscaloosa, Alabama 35486.
Received May 20, 1992

Abstract: Three novel ferrocene–crown derivatives have been prepared along with their previously known amide precursors. The new compounds include 1,1′-(1,4,10,13-tetraoxa-7,16-diazacyclooctadecane-7,16-dimethyl)ferrocene (**2**), *N,N′*-bis(ferrocenylmethyl)diaza-18-crown-6 (**4**), mp 114–116 °C, and bis[*N,N′*-bis(cyclopentadienidylmethyl)-4,13-diaza-18-crown-6]diiron (**6**), mp 104–106 °C. Solid-state structures have been obtained for **2**·H_2O (mp 101–104 °C) and for the $Na^+ClO_4^-$ (mp 208–215 °C dec) and $Ag^+ClO_4^-$ (mp 209–210 °C dec) complexes of **2**. Comparison of these structures shows that the iron atom of ferrocene is a donor ligand for Ag^+ but not Na^+ (the Fe–Ag^+ distance is ≈1 Å shorter than for Fe–Na^+). Stability constants have been obtained in either CH_3OH or CH_3CN with Li^+, Na^+, K^+, Ca^{2+}, and Ag^+ cations. Complexation properties for these compounds have also been assessed by use of fast atom bombardment mass spectrometry. This technique reveals interactions that were not apparent when other analytical methods were applied to these compounds. When the system was studied by electrochemical methods, a new redox couple at more positive potential was observed in the presence of certain alkali, alkaline earth, and transition metal cations. Evidence is presented that cation binding by **2** involves coordination of the cation within the cryptand cavity in contrast to related amides such as **1**. Thus alkali metal redox switching, previously unknown in ferrocenyl amides, is apparent. Evidence is presented for the first example of redox switching of silver ion binding. Determination of the stability constant for the complexation of **2** with the metal cations studied shows a direct correlation with the cyclic voltammetry. The large Ag^+ binding constant and electrochemistry both confirm a direct, stabilizing Ag–Fe interaction. This interaction, previously unknown for kinetically dynamic systems, is confirmed by both ^1H NMR and UV-visible spectroscopy. ^{23}Na NMR studies of compound **2** in the presence of Na^+ show two peaks in the NMR spectrum, corresponding to free and bound Na^+. This behavior is usually associated with cryptands having oxygen donors and suggests that even sodium ions, when bound, are largely encapsulated by compound **2**. This strong interaction permits the first observation of redox switching involving Ag^+ in aqueous solution.

Introduction

The crown ethers and cryptands[1] have afforded the opportunity to make almost infinitely variable synthetic cation transport agents. In many of these systems, such compounds as valinomycin have served as models, and, in a few cases, function near that observed for natural systems has been realized. An entirely different approach has been to imbue unnatural materials with properties that will benefit the cation transport phenomenon.[2] Among these, various switching mechanisms have proved to be the most promising. One of us has recently reviewed this area.[3] Among the chemical subspecies that have served as switches are azobenzene (photochemical switch), phenolic systems (pH switch), nitrobenzene and anthraquinone (neutral → anion redox switch), and ferrocene (neutral → cation redox switch).

In the latter case, the key design principle is that ferrocene has a readily accessible redox couple such that neutral ferrocene can be converted easily into the ferrocenium cation. When the metallocene is incorporated within a cation binding structure, ferrocene's d-electrons may or may not serve as donors for a bound cation, but, when oxidized [Fe(II) → Fe(III)], a repulsive positive charge is placed in proximity to the bound cation. This chemical change diminishes the cation binding capacity of the ligand which is switched from a high to a low binding state. We report here the preparation of a novel ferrocenyl cryptand which exhibits the hoped-for redox switching properties, and we present evidence that complexation occurs within the cavity and not on the periphery as is the case with certain amidic relatives of the present structure.

Results and Discussion

Synthesis and Characterization. The ferrocenyl derivatives described in this paper were all prepared by a similar approach. Ferrocenecarboxylic acid or 1,1′-ferrocenedicarboxylic acid was converted into the acyl or diacyl chloride by treatment with oxalyl chloride. This, in turn was treated with 4,13-diaza-18-crown-6 in a stoichiometric proportion appropriate for synthesis of the desired derivative. Ferrocenyldimethyl[2.2]cryptand was prepared by this sequence, which afforded first the previously reported[4] diamide, **1** [obtained as a yellow-orange solid (mp 180–181 °C) in 43% yield]. Reduction was effected by stirring a mixture of **1** (4 mmol) at ambient temperature under N_2 in 15% by volume tetrahydrofuran (THF) in CH_2Cl_2 (100 mL) with $LiAlH_4$ (16 mmol). These somewhat unusual conditions permitted us to obtain the previously unknown **2**·H_2O (**2** is reported to be an oil[5]) as yellow-orange crystals, mp 101–104 °C. The synthetic steps are shown in Figure 1.

Similar approaches were used in the preparation of BiBLEs **3** and **4** as well as for bis(cryptand)s **5** and **6**, and 1,1′-bis(dimethylaminomethyl)ferrocene (**9**).[6] Cholestanyloxymethylferrocene (**7**),[7] *N,N′*-bis[(1-carbomethoxy)ferrocenylcarbonyl)-4,13-diaza-18-crown-6 (**8**),[8] and *N,N′*-bis(benzyl)-4,13-diaza-18-crown-6 (**10**)[9] were obtained commercially or by the method described in the cited reference. The structures of the compounds involved in the present study are illustrated below.

Mass Spectral Analysis. Fast atom bombardment mass spectrometry (FAB/MS) is a sensitive probe of solution phenomena

[‡] University of Alabama.
Address correspondence concerning mass spectrometry to this author.
§ Address correspondence concerning electrochemistry to this author.
† Address correspondence concerning ligand syntheses and other aspects of the work to this author.

(1) Gokel, G. W. *Crown Ethers and Cryptands*; Royal Society of Chemistry: London, 1991.
(2) Araki, T.; Tsukube, H. *Liquid Membranes: Chemical Applications*; CRC Press: Boca Raton, FL, 1990.
(3) Kaifer, A. E.; Echegoyen, L. A. In *Cation Binding by Macrocyclic Systems*; Inoue, Y., Gokel, G. W., Eds.; Marcel Dekker: New York, 1990, p 363.
(4) Hammond, P. J.; Bell, A. P.; Hall, C. D. *J. Chem. Soc., Perkin Trans. 1* **1983**, 707.
(5) Vögtle, F.; Oepen, G. *Liebigs Ann. Chem.* **1979**, 1094.
(6) Pauson, P. L.; Sandhu, M. A.; Watts, W. E. *J. Chem. Soc.* **1966**, 251.
(7) Medina, J. C.; Gay, I.; Chen, Z.; Echegoyen, L.; Gokel, G. W. *J. Am. Chem. Soc.* **1991**, *113*, 365.
(8) Medina, J. C.; Li, C.; Bott, S.; Atwood, J. L.; Gokel, G. W. *J. Am. Chem. Soc.* **1991**, *113*, 366.
(9) Gatto, V. J.; Gokel, G. W. *J. Am. Chem. Soc.* **1984**, *106*, 8240.

0002-7863/92/1514-10583$03.00/0

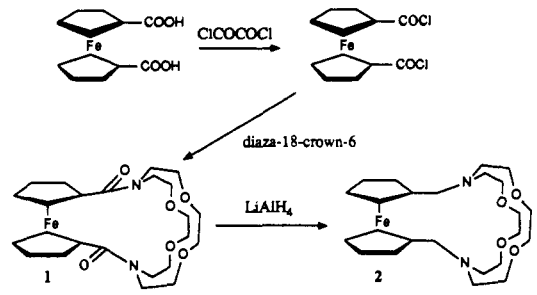

Figure 1. Synthesis of compound **2**.

and may be applied under a variety of conditions. We employed this method to screen a variety of potential host molecules for their ability to bind cations. The FAB/MS technique is operationally simple and its sensitivity makes it economical. Thus a broad survey could be accomplished rapidly with good confidence in the general binding observations. In the FAB/MS technique, a ligand–cation complex formed in a solution matrix may be desorbed by a high energy atom beam. We[10] and others[11] have shown that this method may be used to assess binding interactions in crown ethers and related systems. In the present context, the structures have often proved difficult either to prepare, to purify, or both. The FAB/MS technique is especially useful in this context as very small samples ($\leq$1 mg) may be rapidly screened for ligand/cation interactions.

a. Choice of FAB Matrix. Although several different solution matrices have been explored for use in FAB/MS analyses, we chose *m*-nitrobenzyl alcohol (mNBA) for three reasons. First, of the common solvents used as FAB matrices, mNBA most closely approximates methanol in which solution studies of these compounds were undertaken. Second, our compounds showed good solubility in mNBA. Finally, more data have been determined in this matrix than any other, permitting the broadest range of comparisons.

b. FAB/MS of Compounds 1–6. The compounds studied here fall into three categories. Structures **1–6** are crown or cryptand amides or amines. Compound **7** is an amphiphilic ferrocenyl ether,[7] **8** is a bis(ferrocenyl) receptor developed for small molecule binding,[8] and **9** is a ferrocenyldiamine that was used for comparative purposes. Spectra were obtained for each of these systems on a VG TRIO 2 quadrupole instrument in the absence of any cation. The amides, **1**, **3**, and **5**, all exhibited strong and distinct molecular ions [P$^+$ (used here in place of the more traditional M$^+$ to avoid confusion with M$^+$ = metal ion)] and the protonated molecular ion (P + H)$^+$, in approximately equal intensities. The amines, **2**, **4**, and **6**, exhibited predominantly [P + H]$^+$ but not [P]$^+$ ions, probably reflecting the greater basicity of the amines relative to the amides. Compounds **5** and **6**, each of which contains two macro-rings, exhibited intense [P + 2H]$^{2+}$ ions. These doubly-charged ions were absent in compounds **1–4** which lack the second macrocyclic ring. It seems clear that one charge is in residence on each ring, but we have no direct structural evidence on this issue.

Compounds **7–10** were used for comparison and each had a structural feature of special interest. Compound **7** has a very hydrophobic steroid tail and lacks nitrogen or any other basic atom. In contrast, **9** possesses two basic nitrogen atoms but lacks a macrocycle or a hydrophobic tail. Compound **8** contains four carbonyl groups as does **5** but lacks the second macrocyclic ring. These carbonyl groups might serve as a metal ion binding site rather than the macro-ring. Compound **10** is *N*,*N*′-dibenzyl-

Chart I

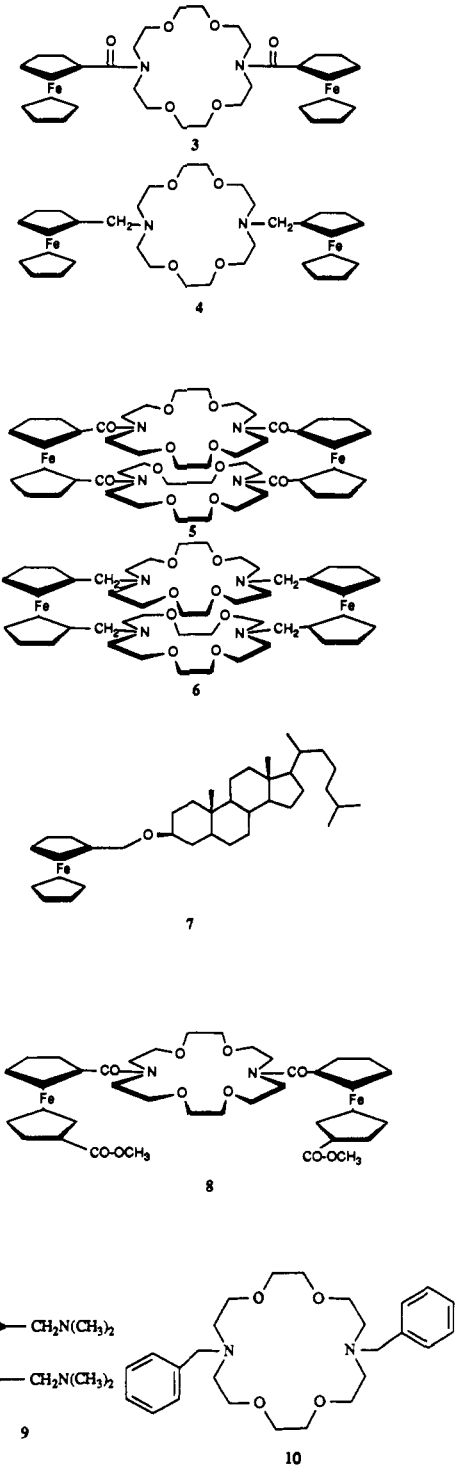

diaza-18-crown-6, which has both nitrogen donors and a macro-ring but lacks the ferrocene residue and any hydrophobic tail or sidearm donor group.

The FAB analysis of **7** produced an intense spectrum in which matrix ions were completely suppressed. Compound **7** was known from previous studies[7] to be surface active; this fact was confirmed by the absence of matrix ions. On the other hand, the spectra of compounds **1–6** contained intense peaks attributable to matrix ions, confirming their much lower surface activity. Compound **8** was selected because it has four amide carbonyl groups and is expected to bind cations more effectively than **3**, which has only two amide carbonyl groups. The FAB spectrum of **8** (unlike surface-active **7**) was characterized by a [P + H]$^+$ rather than a [P]$^+$ peak and exhibited considerable fragmentation. The FAB spectrum of **9** showed extensive fragmentation: ions were observed

(10) Takahashi, T.; Uchiyama, A.; Yamada, K.; Lynn, B. C.; Gokel, G. W. *Tetrahedron Lett.* **1992**, 3825.

(11) (a) Johnstone, R. A. W.; Lewis, I. A. S.; Rose, M. E. *Tetrahedron* **1983**, *39*, 1597. (b) Johnstone, R. A. W.; Rose, M. E. *J. Chem. Soc., Chem. Commun.* **1983**, 1268. (c) Beer, P. D. *J. Chem. Soc., Chem. Commun.* **1985**, 1115. (d) Beer, P. D.; Crane, C. C.; Keefe, A. D.; Whyman, A. R. *J. Organomet. Chem.* **1986**, *314*, C9. (e) Laali, K.; Lattimer, R. P. *J. Org. Chem.* **1989**, *54*, 496. (f) Yamada, K.; Matsutani, S.; Uchiyama, A.; Takahashi, T. *J. Inc. Phenom.* **1991**, *11*, 49.

Table I. Complexation of Sodium and Silver Cations by Amides and Amines Assessed by FAB Mass Spectral Analysis

cpd no.	ratio [P + M]/[P + H] M = Na^+	M = Ag^+
1	0.2	ND
2	4.4	34 ± 5
3	0.1	ND
4	1.9	22 ± 4
5	0.8	ND[a]
5	0.4	ND[b]
6	45	11 ± 2[a]
6	8.0	31 ± 4[b]

[a] Ratio of [P + Na]/[P + H]. [b] [P + 2Na]/[P + 2H]. ND means not detected.

consistent with the loss of $[N(CH_3)_2]$. The molecular ion (P^+) was approximately 20% of the base peak ($P - [N(CH_3)_2]$). Compound **10**, on the other hand, produced a FAB spectrum in which [**10** + H] was the base peak.

c. FAB Analysis of Sodium Cation Binding. Sodium cation was added to nitrobenzyl alcohol as its perchlorate in stoichiometric ratios of 1 to 2 depending on the compound (see Experimental Section). In no case was a substoichiometric amount of Na^+ present nor was the excess ever greater than 100%. The data obtained are summarized in Table I. As is obvious from the data in the table, the amines bind Na^+ much more effectively than do the amides. This is expected since the carbonyl groups rigidify the macro-rings and tend to point away from the cation-binding macro-ring. Notwithstanding this generalization, it is useful to compare and contrast the structures by amide–amine pairs, i.e., **1–2**, **3–4**, and **5–6**. The Na^+ binding of ferrocenylcryptand **2** is about 20-fold greater than that of the amide precursor (**1**). A much smaller difference in binding strength is observed for **3** and **4**, probably because there is no third dimension of binding in either case. Nevertheless, binding by the amine (**4**) exceeds that of the amide (**3**) by about 10-fold. The greatest difference in binding strengths is observed for **5** and **6**. The bis(crown) diamine (**6**) has two macro-rings and two ferrocenes that constitute a semi-flexible box. This can afford one or more bound cations a three-dimensional array of donor groups in either case, but the amide carbonyl groups, once again, are expected to be turned outward and to diminish the basicity of intra-annular nitrogen in **5**.

Compounds **7** and **9** showed as expected no discernible interaction with Na^+ when assessed by the FAB/MS technique. In contrast, **8** showed significant binding to this cation. Moreover, binding of Na^+ by **8** was significantly greater than observed for **3**. The essential difference between **3** and **8** is the presence on the latter of ester functional groups in the 1-positions of each ferrocene. These can rotate toward the macro-ring-bound cation and provide additional solvation in the fashion of bibracchial lariat ethers. Thus, each sodium would be coordinated to four equatorial ether oxygen atoms and two apical ester carbonyl groups.

d. FAB Analysis of Silver Cation Binding. Data obtained by the FAB/MS technique for silver binding by compounds **1–6** are summarized in Table I. Generally, the trends observed for sodium are reflected in the silver binding data except that, in amine compounds **2**, **4**, and **6**, interactions are stronger owing to participation in binding by ferrocenyl iron (vide infra). It is of special interest to note that no interaction was detected between Ag^+ and the much studied[12] carbonyl–ferrocene derivatives **1**, **3**, and **5**.

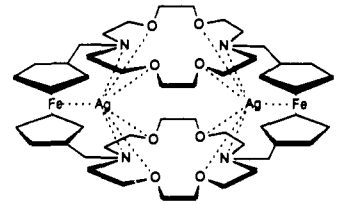

Figure 2. Postulated complex structure of **6**·$(Ag^+)_2$.

Typical spectra for **1**·Ag^+ and **2**·Ag^+ are shown in the supplementary material.

Three interesting and important observations can be made concerning silver binding by the structures surveyed. Compound **9** is devoid of any macro-ring but shows a clear interaction with Ag^+. No evidence for any interaction between **9** and Na^+ was observed. The **9**·Ag^+ interaction was thought to be possible based upon crystal structure data for a structurally related 1,1′-dithioferrocene that forms a stable complex with palladium[13] and because of results obtained for **2**·Ag^+. We therefore assert that a three-point complex forms between **9** and Ag^+ in which the principal donors are iron and two nitrogen atoms. Of course, the FAB/MS method permits us to obtain no structural detail, but it is especially important to note that no such interaction was detected by solution electrochemical methods, further emphasizing the sensitivity and versatility of the FAB/MS technique in studies of this sort.

Since neither the ferrocene nor the benzyl group is normally considered a donor group for alkali metal cations, it might be expected that complexation of either Na^+ or Ag^+ by *N,N′*-bis(ferrocenylmethyl)diaza-18-crown-6 (**4**) and *N,N′*-bis(benzyl)diaza-18-crown-6 (**10**) would be similar, if not identical. Indeed, **4** and **10** bind Na^+ about equally well. Different behavior may well be expected for Na^+ and Ag^+. Silver will be favored by the two nitrogen atoms of either **4** or **10** and may also involve the ferrocenyl sidearms of **4** in a "lariat" interaction with the ring-bound cation. Silver cation is observed to be bound by **10** about 3-fold more strongly than is Na^+ because of the special Ag^+–N interactions, but the complex **4**·Ag^+ is stabilized by about 4- to 5-fold relative to **10**·Ag^+ because of ferrocene's presence.

The final, and perhaps most interesting, observation to emerge from this survey concerns compound **6**. As noted above, significant ion intensities were observed for masses corresponding to $[\mathbf{6}\cdot 2Na]^{2+}$. If a silver–iron interaction is possible as shown for **2**, then two such interactions would be expected in **6**. Indeed, evidence for such a double complex was clearly obtained (see supplementary material). Although we cannot say exactly what is the structure of this complex, we postulate the arrangement shown in Figure 2 based on an examination of CPK molecular models.

Spectral Analysis of Cation Complexation by 2. The possibility of interactions between metal cations and oxygen, nitrogen, and especially iron led us to examine a range of solution spectra. We chose to study a combination of NMR and ultraviolet spectra because these could give direct observations of the bound metal ion in one case (^{23}Na) and the overall electronic situation when binding occurs.

a. ^1H NMR Analysis of 2 Binding Na^+, Ca^{2+}, K^+, and Ag^+. The ^1H NMR spectrum (400 MHz) of **2** in CD_3CN is shown in Figure 3a. The spectrum may be considered essentially in regions δ 2.5–2.7 (NCH_2CH_2O), ≈4.0 and ≈4.2 (ferrocenyl protons), and 3.5–3.8 ppm (crown and N–CH_2). When less than an equivalent of any cation is added, both complexed and uncomplexed species are observed (data not shown) indicating that cation exchange is slow on the NMR time scale. The decomplexation rates, k_d (or k_{-1}) ranged from $k_d \leq 27\ s^{-1}$ for Na^+ to $k_d \leq 280\ s^{-1}$ for Ag^+. The decomplexation rates for Ca^{2+} and K^+ are, respectively, ≤ 178 s^{-1} and ≤ 115 s^{-1} in CD_3CN. The spectra shown in lines b–e of Figure 3 show the effects of 1 equiv each of metal cation. Addition of Na^+, K^+, and Ca^{2+} can be characterized as generally

(12) (a) Hall, C. D.; Sharpe, N. W. *J. Organomet. Chem.* **1991**, *405*, 365. (b) Hall, D. C.; Tucker, J. H. R.; Sharpe, N. W. *Organometallics* **1991**, *10*, 1727. (c) Hall, C. D.; Sharpe, N. W. *Organometallics* **1990**, *9*, 952. (d) Hall, C. D.; Danks, I. P.; Lubienski, M. C.; Sharpe, N. W. *J. Organomet. Chem.* **1990**, *384*, 139. (e) Hall, C. D.; Danks, I. P.; Sharpe, N. W. *J. Organomet. Chem.* **1990**, *390*, 227. (f) Hall, D. C.; Sharpe, N. W.; Danks, I. P.; Sang, Y. P. *J. Chem. Soc., Chem. Commun.* **1989**, 419. (g) Hammond, P. J.; Beer, P. D.; Dudman, C.; Danks, I. P.; Hall, D. C.; Knychala, J.; Grossel, M. C. *J. Organomet. Chem.* **1986**, 306, 367. (h) Beer, P. D.; Elliot, J.; Hammond, P. J.; Dudman, C.; Hall, C. D. *J. Organomet. Chem.* **1984**, *263*, C37. (i) Hammond, P. J.; Beer, P. D.; Hall, C. D. *J. Chem. Soc., Chem. Commun.* **1983**, 1161.

(13) (a) Seyferth, D.; Hames, B. W.; Rucker, T. G.; Cowie, M.; Raymond, S. D. *Organometallics* **1983**, *2*, 472. (b) Cowie, M.; Dickson, R. S. J. *Organomet. Chem.* **1987**, *326*, 269.

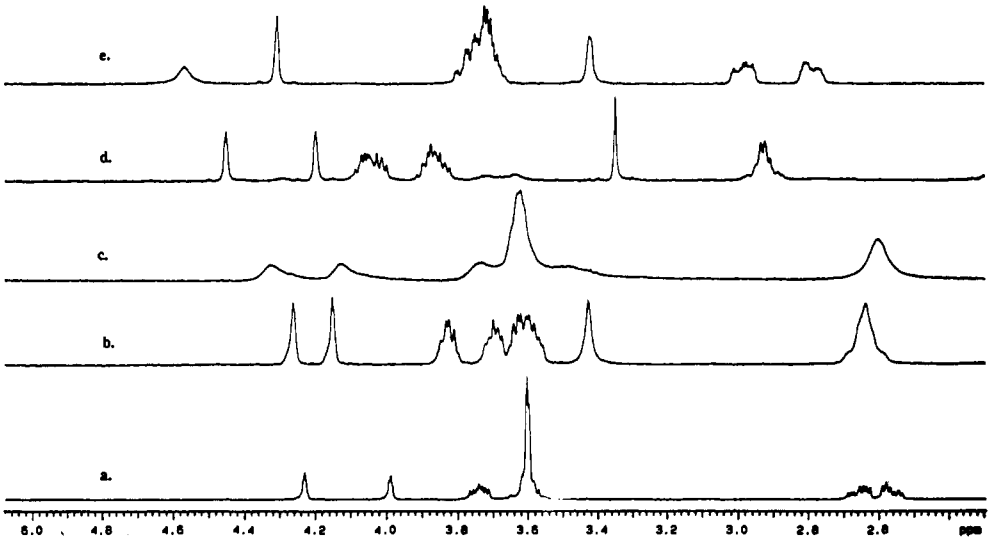

Figure 3. ^{1}H NMR (400 MHz) of **2** in CD_3CN after the addition of 1 equiv of the indicated cation: (a) **2** alone, (b) **2**·$NaClO_4$, (c) **2**·$KClO_4$, (d) **2**·$Ca(ClO_4)_2$, (e) **2**·$AgClO_4$. Ionophore and cation concentration was 6 mM in CD_3CN.

Table II. ^{13}C NMR Chemical Shifts for **2** and Its Cation Complexes

	signal position[a]						
cation	1	2	3	4	5	6	7
none	54.35	55.35	67.51	70.57	70.81	71.41	89.32
Na^+	54.50	56.17	67.91	68.07	69.58	70.17	87.97
K^+	52.94	56.98	68.04	68.25	68.89	70.46	[c]
Ca^{2+}	53.31	54.70	68.33	69.11	70.24	71.04	86.89
Ag^+	56.37	57.98	66.86	68.80	68.91	69.82	[c]
none[b]	53.36	54.06	67.01	69.68	69.81	70.58	87.10

[a] In CD_3CN. [b] In $CDCl_3$. [c] Ipso peak not resolved after 18 h of accumulations.

similar. For Na^+ and Ca^{2+}, the spectrum is changed much more for the latter because it is the same size as the former but has twice the charge. This difference in charge density is reflected in cation binding constants (in CH_3CN): log $K_S(Na^+)$ = 6.28 and log $K_S(Ca^{2+})$ = 7.16. Potassium cation has the weakest binding constant in the group (log K_S = 5.13) and the spectra show broadening characteristic of slow exchange.

The ^{1}H NMR spectrum of **2** in the presence of Ag^+ is different from the others. Two observed changes are notable. When Ag^+ is present, large shifts are observed for the ferrocenyl protons (the aromatic protons observed at approximately 4.0 and 4.2 ppm in **2** shift to about 4.3 and 4.6 ppm) and the $>NCH_2-$ macro-ring protons shift from ≈2.6 ppm to about 2.9 ppm although the other aliphatic protons are affected little. For the alkali and alkaline earth metal cations, the changes in the proton NMR spectra correlate qualitatively with the cation's charge density, i.e., Ca^{2+} > Na^+ > K^+. In the presence of 1 equiv of Ca^{2+}, the broad resonances observed at about 3.6 and 3.8 ppm in uncomplexed **2** move to ≈3.8–4.0 ppm. The shifts in these broad bands are largest in the presence of Ca^{2+} and also vary in the presence of Na^+, but only small changes are observed in these bands when Ag^+ is added. Two inferences can be drawn from these observations. First, for the alkali and alkaline earth metal cations, coordination is dominated by the crown macroring. For silver, however, the interaction between **2** and Ag^+ involves the ferrocenyl residue and the nitrogen atoms to a greater extent (and perhaps the macroring oxygens to a lesser extent) than for the other cations.

b. ^{13}C NMR Analysis of 2 Binding Na^+, Ca^{2+}, K^+, and Ag^+. Carbon-13 chemical shift data for all of the complexes, determined in deuterated acetonitrile, are shown in Table II. The final line shows the chemical shifts for uncomplexed **2** in $CDCl_3$. We have, by a series of decoupling experiments, assigned the resonances in this latter case. The ferrocene resonances are C-2, 67.01; C-3, 69.81; and ipso, 87.10. The Fc–CH_2 shift is 53.36. The remaining resonances are assigned as $-N[CH_{2(1)}CH_{2(6)}OCH_{2(4)}-]_2$ in which the parenthetical numbers refer to positions in Table II. We have not made these assignments in CD_3CN (as done for $CDCl_3$) nor have we assigned signals to specific carbons when cations are present because, especially in the latter case, shifts are often small. Nevertheless, the high symmetry of these systems is apparent in all of the cases studied (see Figure 4).

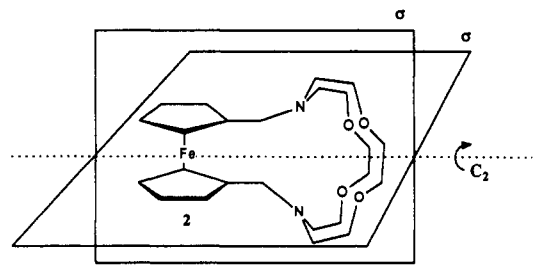

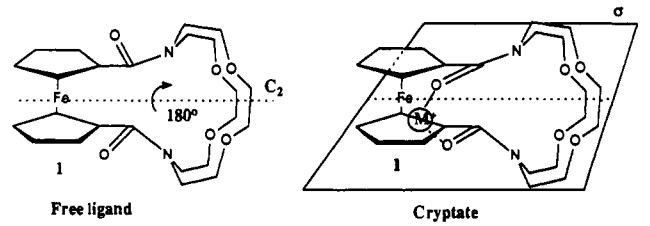

Figure 4. Symmetries of cryptands **1** and **2**.

The amide precursor to **2**, i.e., **1**, has been extensively studied by NMR methods. The normal observation in those cases is a 12-line spectrum. The amide carbonyl groups are assumed to be on opposite sides to the molecular symmetry is C_2.[4] The reasonable argument advanced is that, when a spherical cation is complexed, both carbonyl groups turn to the same side of the molecule (to act as donors) so that, although the C_2 axis is lost, a plane of symmetry bisects the iron atom and the most remote part of the macro-ring.[12a,b] In our case, the observation of seven lines indicates an even higher symmetry: all carbon atoms of an equivalent type share a common resonance position. This suggests that two perpendicular planes of symmetry exist in **2**. This symmetry is obviously not disturbed by inclusion complexation of a spherical cation. An interesting consequence, inter alia, of the higher symmetry exhibited by **2** over **1** is the greater cation binding strength of the former discussed below.

c. ^{23}Na NMR Analysis of 2 Binding Na^+. Relatives of **2** that have been studied previously[12] have contained amide residues attached to ferrocene rather than methylene units. We believed

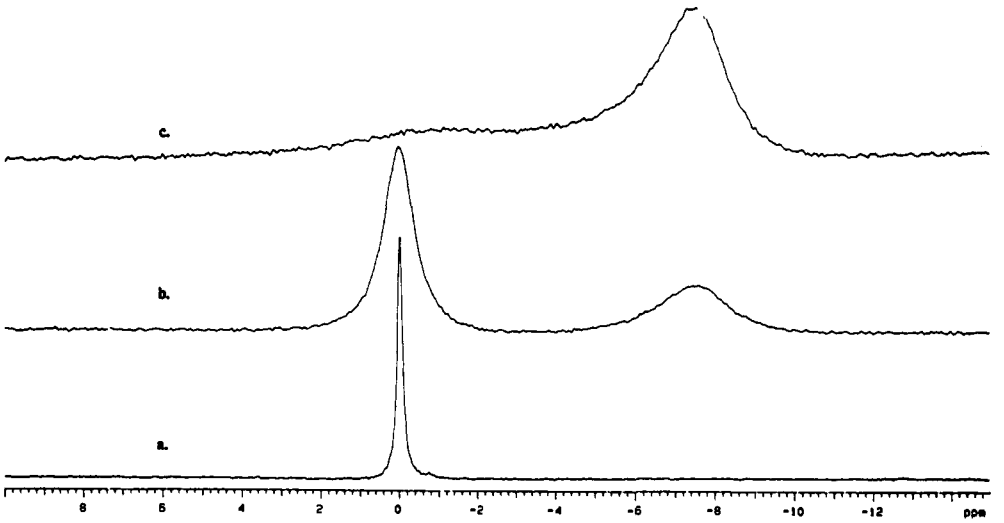

Figure 5. ^{23}Na NMR (105.8 MHz) of NaCl in CD_3OD: (a) 1 mM NaCl in the absence of **2**; (b) in the presence of 1 mM NaCl and 0.5 mM **2**; (c) in the presence of 1 mM NaCl and 1 mM **2**.

that these powerful donor groups not only served to bind cations on the ligands' exterior, but also rigidified these ligands to such an extent that internal complexation was difficult. If **2** differed from these amides by having an internal cavity as we proposed, then it should be possible to observe cation bound within the cryptand versus that in bulk solution. We thus undertook a study of complexation using ^{23}Na NMR. Typical results are shown in Figure 5.

In the presence of excess Na^+, we observed two, resolved Na^+ peaks corresponding to the free and bound species. This behavior is typical of cryptands and rarely observed with crowns.[14,15] Thus, the presumption of internal rather than "surface" interaction is confirmed. The observation of two peaks also shows that the decomplexation rate is relatively slow ($k_{decomplex} \leq 560\ s^{-1}$ in CH_3CN and $k_{decomplex} \leq 1700\ s^{-1}$ in CH_3OH). These facts both substantiate the assumption that **2** is cryptand-like in its neutral binding behavior.

d. Ultraviolet Spectral Analysis of 2. It is reasonable to expect that the iron d-electrons could serve as a donor group. It has been known for many years that the α-ferrocenylmethyl carbocation ($Fc–CH_2^+$) is more stable even than Ph_3C^+, a fact attributed to iron d-orbital interactions.[16] In the case of silver cation, the interaction should be even more favorable since the overlapping orbitals are closer in size when carbon is involved. To our knowledge, this interaction is unknown in kinetically dynamic systems such as **2**. To confirm this iron donor group effect, the complexation of Ag^+ by **2** was examined using UV–visible spectroscopy among other techniques.

Since this interaction is an electronic effect, the best evidence was expected to come from UV–visible spectroscopy. The spectrum of **2** was studied in both acetonitrile and anhydrous methanol in the range 350–600 nm in the absence of any cation and in the presence of Li^+, Na^+, K^+, Ca^{2+}, and Ag^+ (see Figure 6). In all but the latter case, λ_{max} was observed in the range 440–448 nm. In striking contrast to this, **2**·Ag^+ showed a maximum at 460 nm, exhibiting a much larger cation-induced bathochromic shift. These results are consistent with an orbital–orbital interaction between the bound silver cation and the ferrocene d-electrons. Thus the iron atom of ferrocene is a novel and effective donor group in this cryptand, a fact that may have very broad implications.

Cation Binding Studies. Cation binding affinities were determined potentiometrically in homogeneous solution for both **1** and **2** for a variety of cations. Slightly different techniques were used in methanol and acetonitrile, and the methods are detailed in the Experimental Section. It should be noted that some of the values were obtained using a competition technique; these are identified in Table III (see Experimental Section). Ion selective electrodes were used in methanol for the determination of Li^+, Na^+, and K^+.[17]

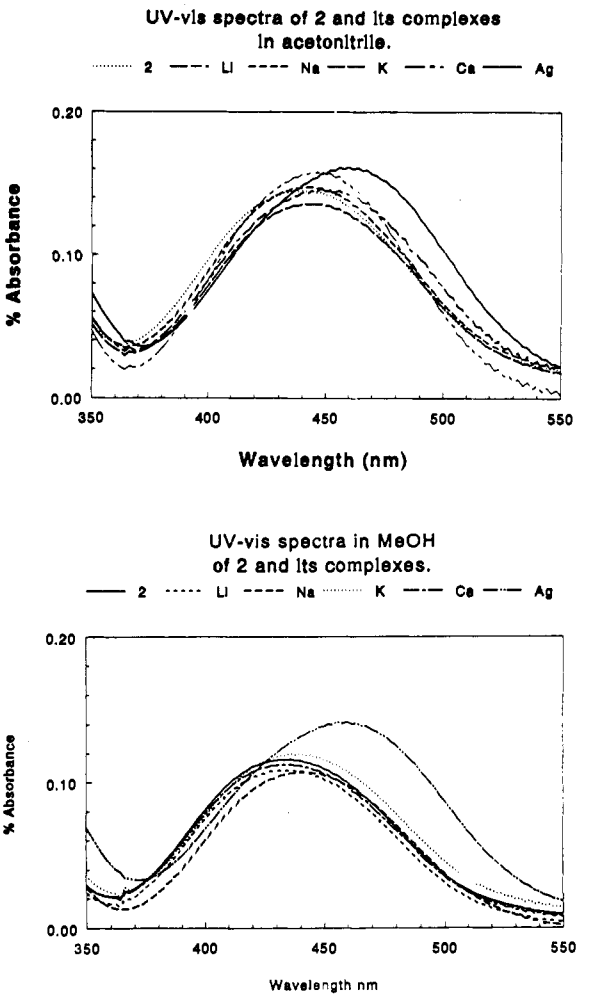

Figure 6. UV–visible spectra of **2** in CH_3CN and MeOH at 1 mM after the addition of 1 equiv of $LiClO_4$, $KClO_4$, $Ca(ClO_4)_2$, and $AgNO_3$.

(14) Detellier, C. In *Modern NMR Techniques and Their Application in Chemistry*; Popov, A. I., Hallenga, K., Eds.; Marcel Dekker: New York, 1991; Chapter 9.
(15) Lin, J. D.; Popov, A. I. *J. Am. Chem. Soc.* **1991**, *103*, 3773.
(16) (a) Richards, J. H.; Hill, E. A. *J. Am. Chem. Soc.* **1959**, *81*, 3484. (b) Trifan, D. S.; Bacskai, R.; *Tetrahedron Lett.* **1960**, *13*, 1. (c) Hill, E. A.; Richards, J. H. *J. Am. Chem. Soc.* **1961**, *83*, 3840. (d) Hill, E. A.; Richards, J. H. *J. Am. Chem. Soc.* **1961**, *83*, 4261.
(17) (a) Frensdorff, H. K. *J. Am. Chem. Soc.* **1971**, *93*, 600. (b) Arnold, K. A.; Gokel, G. W. *J. Org. Chem.* **1986**, *51*, 5015.

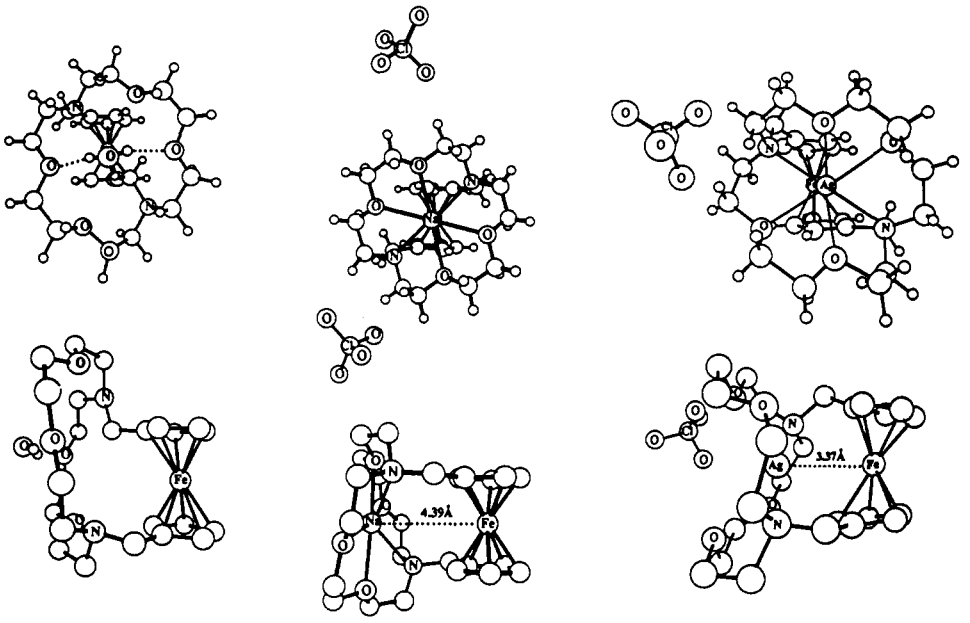

Figure 7. Front and side views of the solid-state structures of $2 \cdot H_2O$, $2 \cdot NaClO_4$, and $2 \cdot AgClO_4$.

Table III. Stability Constants for 1 and 2 at 25.0 °C

ligand	cation	solvent[a]	log K_S
1	Na^+	CH_3OH	1.5
1	K^+	CH_3OH	2.2
1	Ca^{2+}	CH_3CN	4.13[c]
2	Li^+	CH_3CN	3.74[b]
2	Na^+	CH_3CN	6.28[b]
2	K^+	CH_3CN	5.13[b]
2	Ca^{2+}	CH_3CN	7.16[b]
2	Ag^+	CH_3CN	8.35
2	Na^+	CH_3OH	3.72
2	K^+	CH_3OH	3.77
10	Na^+	CH_3OH	2.68
10	Na^+	CH_3CN	5.68[d]
10	K^+	CH_3OH	3.38

[a] Acetonitrile contains 0.1 M Bu_4NPF_6. [b] Values determined by using a competition technique (see Experimental Section). [c] Value from ref 12f. [d] Value from ref 18.

Values in acetonitrile were obtained by monitoring the Ag^+ ion concentration with a silver electrode.[18] In the latter solvent, tetrabutylammonium hexafluorophosphate was present as electrolyte to render conditions as nearly identical as possible with those used in the voltammetry experiments.

The data summarized in Table III can be grouped into three categories. First, two solvents, methanol and acetonitrile, have been used. Second, three types of cations have been studied. These are the alkali metals (lithium, sodium, and potassium), an alkaline earth metal (Ca^{2+}), and silver cation. Third, three different ligands (**1**, **2**, and *N,N'*-dibenzyl-4,13-diaza-18-crown-6, **10**) have been used as binders.

The structural differences between **1** and **2** are clearly manifested in the cation binding behavior. A comparison of their sodium and potassium cation binding strengths in methanol solution is informative. Although neither **1** nor **2** is particularly selective for one cation over the other, the difference in binding strengths is significant. Compound **1**, which is expected not to have a good binding cavity (see above), shows log K_S values of 1.5 (i.e., $10^{1.5}$) and 2.2 respectively for Na^+ and K^+. In contrast, these values are 3.72 and 3.77 for **2**. The binding values recorded are compared to those obtained for *N,N'*-dibenzyl-4,13-diaza-18-crown-6, (**10**), an obvious analogue of **2**. Sodium cation binding differs some between **2** and **10**, but the difference between **1** and **10** is much more striking, although expected.[18] Likewise, K^+ binding by **1** stands out by being much less than the similar values observed for **2** and **10**.

Methanol and acetonitrile have similar polarities but differ in both hydrogen bonding ability and donicity. In general, crown ethers and cryptands are found to exhibit higher binding constants in CH_3CN than in CH_3OH for the same cations. This is due to a combination of effects that have been discussed elsewhere.[19] Nevertheless, the same trend is observed in the present case. Thus, Na^+ and K^+ binding constants (log K_S) are 2–3 decades higher in acetonitrile than in methanol. We have previously observed a similar trend with a series of *N,N'*-disubstituted-4,13-diaza-18-crown-6 derivatives.[18]

Three of the cations studied can be considered special cases. These are Li^+, Ag^+, and Ca^{2+}. The K_S value observed for Li^+ is large in acetonitrile, but smaller than for either Na^+ or K^+. This trend is expected. Silver cation generally shows highest cation binding with ligands that have nitrogen atom donors disposed at 180° angles and at a distance appropriate for Ag^+. Compound **2** has two nitrogens so disposed and at a distance of 5.5 Å ($2 \cdot H_2O$).[20] The ionic radius of silver(I) is 2.8 Å making it the right size to be effectively bound by **2**, and the log K_S value observed, 8.35 in CH_3CN, is substantial. An important observation is that the affinity of **2** in acetonitrile is significantly larger for Ag^+ than for K^+ ions ($\Delta\Delta G_{Ag^+-K^+} = -4.4$ kcal/mol). The reverse might be expected for compounds of this type since CH_3CN is a better solvating agent for Ag^+ ions. This is best observed in the selectivity of [2.2.2]cryptand in which case K^+ is selected over Ag^+ (where $\Delta\Delta G_{Ag^+-K^+} = +2.5$ kcal/mol). We believe that this discrepancy in selectivities is due in large part to increased solvation in the $2 \cdot Ag^+$ complex created by the interaction between the d-orbitals of both metals. This type of interaction would be weak or absent in the $2 \cdot K^+$ complex.

The large magnitude of the binding constant of **2** with Ca^{2+} compared to either Na^+ or K^+ is due in part to the greater solvation demand made by Ca^{2+} relative to Na^+ or K^+. In particular, the ionic radius of both Na^+ and Ca^{2+} is 1.95 Å, but the higher charge in the latter makes its solvation enthalpy greater. We consider the binding behavior in the group Na^+, K^+, and Ca^{2+} to be controlled by differences in charge density and to involve forces fundamentally different from those that operate when Ag^+ is bound.

(18) Gustowski, D. A.; Gatto, V. J.; Mallĕn, J. V.; Echegoyen, L.; Gokel, G. W. *J. Org. Chem.* **1987**, *52*, 5172.

(19) Izatt, R. M.; Bradshaw, J. S.; Nielsen, S. A.; Lamb, J. D.; Christensen, J. J.; Sen, D. *Chem. Rev.* **1985**, *85*, 271.

(20) Medina, J. C.; Goodnow, T. T.; Bott, S.; Atwood, J. L.; Kaifer, A. E.; Gokel, G. W. *J. Chem. Soc., Chem. Commun.* **1991**, 290.

Table IV. Selected Bond Distances for Ferrocenyl[2.2]cryptand Complexes

	bond angle (deg) or distance (Å)			
atoms involved	**1**·2H_2O[a]	**2**·H_2O	**2**·Na^+	**2**·Ag^+
Fe–C	2.037 (2)	2.049 (1)	2.04 (0.4)	2.04 (3)
inter-ring dist	3.286	3.303		
C_5H_5 ring tilt (deg)	0.4	0	0	10
C–C (cp)	1.425 (1)	1.416 (3)	1.40 (1)	1.40 (2)
$C–C_{(O-C-C-O)}$	1.464 (6)	1.482 (8)	1.44 (1)	1.50 (1)
$C–C_{(N-C-C-O)}$	1.515 (1)	1.504 (3)	1.49 (14)	1.51 (1)
$C–C_{(Fc-C)}$	1.483 (10)	1.502 (4)	1.50 (1)	1.51 (14)
$C–O_{(ether)}$	1.420 (1)	1.419 (8)	1.40 (2)	1.41 (2)
$C–N_{(macro-ring)}$	1.479 (1)	1.469 (4)	1.50 (3)	1.46 (3)
$C–N_{(Fc-C-N)}$	1.337 (5)	1.475 (12)	1.52 (1)	1.48 (17)
C=O	1.225 (1)			
$M^+–N_1$			2.86 (1)	2.37 (1)
$M^+–N_2$			2.36 (1)	
$M^+–O_{1A}$			2.53 (1)	2.76 (1)
$M^+–O_{1B}$				2.80 (1)
$M^+–O_{2A}$			2.54 (1)	2.94 (1)
$M^+–O_{2B}$				2.60 (1)
M^+–Fe			4.387 (4)	3.37 (2)
N→N	5.2	5.5		

[a] Data from ref 22.

Solid-State Structures. Compound **1**, the bis(amide) precursor to **2**, was prepared by Hall and co-workers who obtained the solid-state structure of **1**·2H_2O. Uncomplexed **2** was prepared by Vögtle as an oil. When hydrated, however, **2**·H_2O is crystalline. Solid-state structures for **2** in the presence of complexing water, Na^+, and Ag^+ have all been obtained, and ORTEP plots are shown in Figure 7. The structure of **2**·H_2O was reported in preliminary form[20] but without the details summarized in Table IV.

The much-studied diamide (**1**) precursor to ferrocenyl[2.2]-cryptand **2** differs substantially from the latter owing to the presence of its two carbonyl groups. The carbonyl groups of **1** are potent donor groups. Because of amide resonance and conjugation, the carbonyl groups are, in each case, essentially parallel with the ferrocenyl aromatic ring. This undoubtedly enhances extra-cavity binding but also contracts the internal binding cavity. The extensive studies of Hall, Beer, and co-workers, suggest that the carbonyl groups do, indeed, dominate the binding as expected from this structure.

Thus, **2** is the first example of a cryptand-like system containing a single ferrocene that binds metallic cations within its cavity rather than externally. The solid-state structure of **2**·H_2O shows clearly that a cavity is present in this compound and that ample room is available within the cavity to bind various cations. Evidence for this can easily be found in the N–N distance observed for the diaza-18-crown-6 subcyclic unit. In **2**·H_2O, the N–N distance is 5.5 Å. The corresponding distance observed (solid-state structure) in diaza-18-crown-6[21] is 5.8 Å while this span is only 5.2 Å in diamide **1**.[22] In order to maintain planarity of the >N–CO–Fc linkage, the macro-ring must pucker outward. This is not a requirement in the saturated analogue, and the more extended ring structure may be attributed to it.

When Na^+ is bound by **2**, the macro-ring adjusts to what may be considered a "normal" binding conformation in which O–Na^+ distances are in the range 2.53–2.54 Å. In known complexes of lariat ethers and cryptands, distances are typically in the range 2.5 ± 0.1 Å. For example, in the Na^+ complex of *N*-carboxymethylaza-15-crown-5, the four ring O–Na^+ distances are 2.48 Å, 2.51 Å, 2.52 Å, and 2.62 Å. The average O–Na^+ distance in the Na^+ complex of [2.2.1]cryptand is 2.48 ± 0.04 Å. The $M^+–N_{ring}$ distances in **2**·Na^+ are 2.36 Å and 2.86 Å, indicating that the ring is distorted. Note that the average of these distances is 2.61 Å and that the N–Na^+ distances in [2.2.1] are in the range 2.65 ± 0.06 Å. An additional important observation about complex **2**·Na^+ is that the Fe–Na^+ distance is 4.39 Å, too long for any direct interaction to be invoked.

If the sodium complex of **2** holds few surprises, the silver complex abounds in them. First, the macro-ring is strongly distorted. The average C–C bond distances in the crown macro-ring are nearly as long as in the noncomplexing **1** or the externally complexed **2**·H_2O. The implication is that the C–C bond contraction expected when an electron-withdrawing Lewis acid binds adjacent oxygen is absent. This suggests a stronger interaction for other donors within the ligand sphere. Foremost among these must be the N–Ag^+–N interactions, well known to be strong. The Ag^+–N distances (2.37 Å) are substantially shorter than observed in [2.2.2]cryptand (2.48 Å). The Ag^+–O distances of **2**·Ag^+ are longer (2.67 Å, 2.80 Å) than observed (2.73 Å) for the [2.2.2] complex. This suggests a strong interaction between silver and nitrogen.

The most dramatic evidence for a special interaction in this system involves ferrocene itself. Although the ionic diameter of Ag^+ (2.6 Å) is considerably larger than that of Na^+ (1.95 Å), the Fe–Ag^+ distance is 3.37 Å, while the Fe–Na^+ distance is more than 1 Å longer. Indeed, the two cyclopentadienide rings are tilted by 10° in the silver complex and completely planar in the sodium complex. We conclude that there is a direct, stabilizing Fe → Ag^+ interaction.

A possible explanation of these observations that does not invoke a direct iron–silver interaction is that the shortened silver–iron distance is an artifact of the strong silver–nitrogen interaction. This may, in part, be true, but it does not account for the tilted cyclopentadienyl rings. The energy cost of these ring tilts must be compensated by an enhanced stabilization resulting from silver–iron proximity. Although such an interaction is unknown in a dynamic system such as that described here, precedence[13] for it has been noted above. In this case, an Fe–Pd bond distance of 2.878 Å was observed, and the two cyclopentadienyl rings were distinctly tilted to allow approach of Pd.

Taken together with the mass spectra, electronic spectra, and the proton, carbon, and sodium NMR, it seems inescapable that there is a hitherto unreported, direct interaction between silver cation and ferrocenyl iron that imparts special properties to this redox-switchable complex.

Cyclic Voltammetric Studies. One of the most interesting attributes of ligand **2** is the presence of a ferrocenyl redox-active group in proximity to the cation binding site. This feature suggests that binding and electron transfer events can influence one another owing to the short distance between their respective sites. Binding events could then affect the thermodynamics and kinetics of electron transfer reactions on the ferrocenyl subunit. Conversely, the oxidation state of the ferrocenyl subunit may change the cation binding affinity of the neighboring macrocycle. Similar concepts have been demonstrated with a number of redox-active macrocyclic ligands having nitrobenzene, anthraquinone, and other electroactive groups in their structures. The term redox-switchable ligands has been coined to describe this versatile class of cation hosts. In principle, cyclic voltammetry (CV) of the ligand in the presence of variable concentrations of the metal ion of choice affords a simple and effective way for estimating the communication between the redox and binding sites. In the following sections we describe the relevant CV data obtained with ferrocenyl derivatives **1**–**9**.

a. Cyclic Voltammetry of 2 in the Presence of Metal Cations. CV of a 1.0 mM solution of ligand **2** in CH_3CN/0.1 M $TBA^+PF_6^-$ yields a single set of waves centered at 0.216 V versus SSCE that corresponds to the reversible oxidation of the ferrocene moiety (see Figure 8A). The difference between the peak potentials (60 mV) and the linear dependence of the anodic peak current with the square root of the scan rate clearly establish the expected reversible character of this redox couple. Addition of substoichiometric concentrations of $NaClO_4$ to the same solution results in the appearance of a new set of redox waves at 0.402 V versus SSCE (see Figure 8B). The currents for the new redox couple increase linearly with the concentration of Na^+ ion until a full equivalent is added; at this point, the original set of waves disappears and the new redox couple reaches full development. This

(21) Herceg, M.; Weiss, R. *Bull. Soc. Chim. Fr.* **1972**, 549.
(22) Beer, P. D.; Bush, C. D.; Hamor, T. A. *J. Organomet. Chem.* **1988**, *339*, 133.

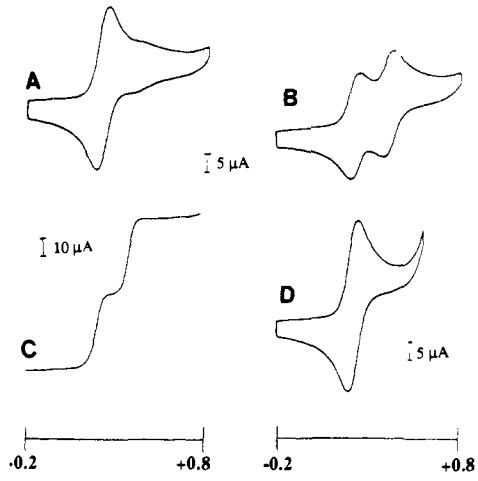

Figure 8. Voltammetric response of acetonitrile solutions containing 1.0 mM **2**: (A) stationary glassy carbon electrode (0.08 cm^2), scan rate = 100 mV/s; (B) same conditions as (A) with 0.5 mM $NaClO_4$ added; (C) solution conditions as in (B), glassy carbon electrode (0.196 cm^2) rotating at 1000 rpm; (D) same conditions as in (B) with 2.5 mM [2.2.1]cryptand added.

indicates that the second set of waves results from the reversible oxidation of the ferrocenyl subunit in the **2**·Na^+ complex. This assignment is further confirmed by addition of a 5-fold excess of cryptand [2.2.1] to the system. This ligand, which forms a very stable Na^+ complex, binds all the Na^+ ions in the solution, releasing free **2** as concluded from the full reappearance of the original redox couple at 0.216 V (see Figure 8D). This observation verifies that Na^+ complexation by **2** is a fully reversible process, although it does not provide detailed information about the kinetics of complexation.

The electrochemical behavior observed for **2** in the presence of substoichiometric amounts of Na^+ ion is quite unusual since the interaction between an electroactive species and an additive usually shifts the observed half-wave potential; i.e., the potential shifts gradually as the concentration of the interacting additive increases until a saturation value is reached. This latter value is ascribed to the half-wave potential of the corresponding complex species. The behavior observed with **2** and Na^+ ion is fundamentally different since two redox couples are clearly observed for Na^+ concentrations within the range $0 < [Na^+] < [\mathbf{2}]$. Since the decomplexation kinetics of internal metal–cryptand complexes are usually quite slow, it could be argued that the shape of the voltammogram is controlled by kinetic effects. However, the voltammograms do not seem to show any kinetic effects. For instance, the shape of the CV of Figure 8B remains unaltered from 0.02 to 5 V/s, a wide range of scan rates. This suggests that, if the rate of decomplexation (or complexation) actually influenced the voltammograms, the time scale of our voltammetric experiments is either much shorter or much longer than the lifetime of the relevant species. Furthermore, Figure 8C shows the current–potential trace obtained with a rotating disk electrode in which two waves are also clearly observed. These two waves correspond exactly to the two sets of peaks recorded in the CV experiments. Again, the resolved, *two-wave* voltammetric behavior seems to be independent of the experimental time scale as it is equally observable in both transient (CV) and steady-state (rotating disk voltammetry) experiments.

Two factors seem to be responsible for the observation of two resolved redox couples under the conditions of Figure 8B: first, the large difference between the half-wave potentials for the two observed redox couples that we assign to the process $\mathbf{2} - e^- \rightarrow \mathbf{2}^+$ and $\mathbf{2}\cdot Na^+ - e^- \rightarrow (\mathbf{2}\cdot Na)^{2+}$; second, the high equilibrium binding (stability) constant for the **2**·Na^+ complex. The large binding constant for the **2**·Na^+ complex keeps this species in the solution while the potential is scanned across the $\mathbf{2} \rightarrow \mathbf{2}^+$ wave (see Figure 2 in supplementary material). As the potential becomes sufficiently positive to oxidize the complex, **2**·Na^+ is present at a concentration level which is essentially equal to that at the beginning of the scan so that a new oxidation wave develops exhibiting peak currents that reflect approximately the stoichiometric fraction of complex in the solution. Therefore, the observation of two resolved redox couples—corresponding to the free and bound forms of the ligand—can be rationalized without using any kinetic considerations. Indeed, the observation of *two-wave* behavior requires a high binding constant for the **2**·Na^+ complex. This type of behavior has been described previously.[23]

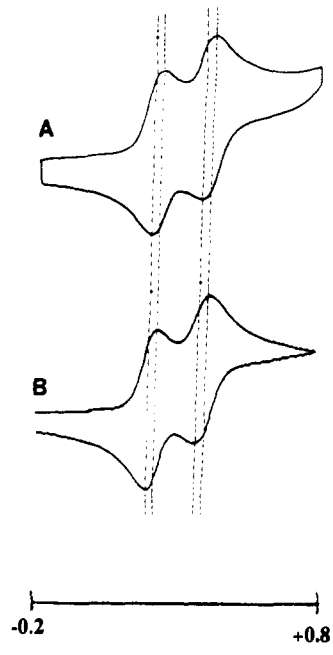

Figure 9. Voltammetric response of a solution containing 1.0 mM **2** and 0.5 mM $NaClO_4$: (A) experimental voltammogram at 100 mV/s; (B) simulated voltammogram obtained using $K = 2 \times 10^6$ M^{-1} and $K_+ = 50$ M^{-1}.

We have successfully simulated the electrochemical behavior of **2** in the presence of substoichiometric concentrations of Na^+. In these simulations, we did not utilize any kinetic assumptions. In fact, the digital simulation program assumed that all the chemical and electrochemical equilibria were fast on the time scale of the experiment so that all equilibria were maintained at all points throughout the simulation. Other assumptions for the simulations are specified in the Experimental Section. The good fit between the simulated and the experimental voltammograms is shown in Figure 9.

Therefore, although the rates of decomplexation of cryptand–ion complexes are typically very slow, the resolved two-wave voltammograms observed with **2** in the presence of Na^+ ion can be explained even if the time scale of the voltammetric experiment is long enough to allow the full equilibration of the complexation process. It is entirely possible that, at fast scan rates, the voltammograms exhibit two-wave shapes due to slow decomplexation kinetics (this is equivalent to saying that the complexation equilibria are *frozen* during the fast voltammetric scan). However, even at slow scan rates, similar voltammetric patterns are observed as a result of the high equilibrium association constant of the **2**·Na^+ complex.

Qualitatively similar voltammetric behavior is observed for **2** in the presence of K^+ ion. However, the difference ($\Delta E_{1/2}$) between the half-wave potential for the oxidations of the **2**·K^+ complex and the free ligand **2** is smaller than in the case of Na^+ ion (see data in Table V). This suggests that $\Delta E_{1/2}$ results from

(23) Charlot, G.; Badoz-Lambling, J.; Trémillion, B. *Electrochemial Reactions*; Elsevier: Amsterdam, 1962; pp 46–50.

Table V. Electrochemical Data[a] for **2** in the Absence and in the Presence of Several Cations

cation	equiv	$E°$	$E°_{ox}$	$\Delta E°$	K/K_+[b]
none	0	0.216			
Li^+	0.5	0.210			
Na^+	0.5	0.214	0.402	0.188	3×10^4
K^+	0.5	0.224	0.348	0.124	4×10^3
Ca^{2+}	0.5	0.214	0.488[c]	0.274	2×10^5
Ag^+	0.5	0.214	0.496	0.282	2×10^5

[a] $E°$ and $E°_{ox}$ are the apparent half-wave potentials of the free ligand and the specified metal ion complex, respectively, as measured in the presence of 0.5 equiv of metal ion. The values are given in V versus SSCE. $\Delta E°$ is the difference between these two values. [b] K and K_+ represent the metal ion binding constants of the reduced and oxidized forms of the ligand, respectively. The K/K_+ ratios given were obtained by optimizing the fit of experimental and simulated voltammograms. [c] This redox couple exhibited a marked degree of electrochemical irreversibility.

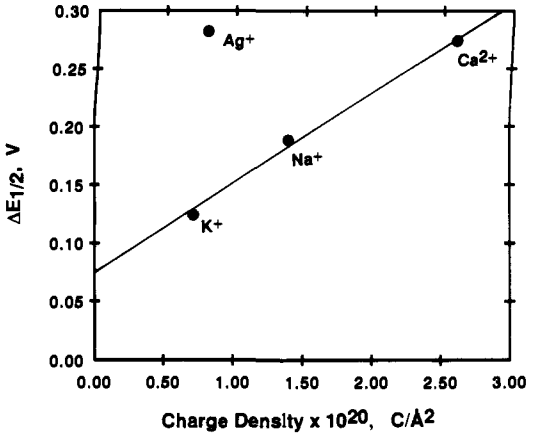

Figure 10. Complexation-induced change in the half-wave potential for the oxidation of **2** as a function of the charge density of the complexed cation.

the electrostatic repulsion effect between the macrocycle-bound cation and the electrogenerated positive charge on the oxidized form of the ferrocenyl subunit. The magnitude of $\Delta E_{1/2}$ is determined by the charge-to-size ratio of the bound cation. Thus, it is higher with Na^+ ion than with the larger K^+ ion. This trend is also followed by the Ca^{2+} ion, which has a charge-to-size ratio approximately twice as large as that of Na^+. However, the oxidation of the Ca^{2+} complex of **2** is not electrochemically reversible. A plot of $\Delta E_{1/2}$ values versus charge-to-size ratio for the cations Ca^{2+}, Na^+, and K^+ is perfectly linear (see Figure 10). We did not perform many experiments with Li^+ since this cation has a much smaller effect on the voltammetric behavior of **2**, probably a reflection of the lower binding constant of the **2**·Li^+ complex.

The electrochemical behavior of **2** in the presence of Ca^{2+}, Na^+, and K^+ clearly indicates that cryptand **2** acts as a redox~ switchable ligand with all three ions. A schematic representation of the equilibria involved is shown in Figure 11. In summary, the oxidation of **2** to 2^+ substantially decreases the binding constant of the ligand for a given cation. The ratio between the two binding constants (K/K_+) increases with the charge-to-size ratio of the bound cation. Compound **2** is the first reported ligand whose voltammetric behavior is greatly affected by alkali metal cations in a relatively polar solvent, such as acetonitrile. Previous reports on other ferrocenyl-based, redox-active ligands demonstrated electrochemical behavior that changed appreciably in the presence of divalent or trivalent cations but was unaltered by the presence of monovalent cations.[12f] Saji also reported a strong influence of Na^+ on the voltammetry of a ferrocene-based crown ether using a less polar solvent, such as dichloromethane.[24] Thus, cryptand **2** appears to be a better ligand for cations than previously reported

(24) (a) Saji, T.; Kinoshita, I. *J. Chem. Soc., Chem. Commun.* **1986**, 716. (b) Saji, T. *Chem. Lett.* **1986**, 275.

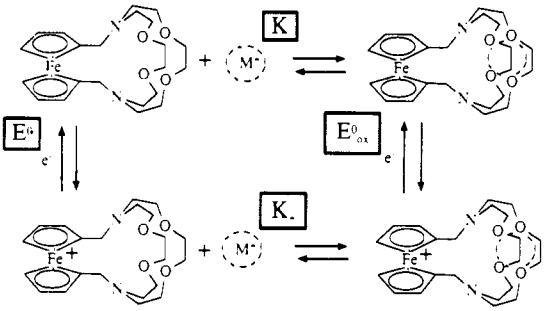

Figure 11. Binding scheme.

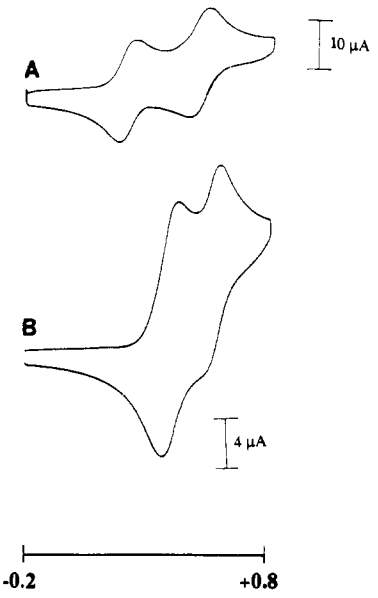

Figure 12. Voltammetric response at 100 mV/s of ferrocenyl-based ligands in the presence of Ag^+ ion: (A) 1.0 mM ligand **2** + 0.5 mM Ag^+; (B) 0.5 mM ligand **6** + 0.5 mM Ag^+. Solvent system: MeCN/0.1 M $TBA^+PF_6^-$.

ferrocene-containing hosts. The unique structural feature of compound **2** is its well-formed cavity which facilitates the formation of internal metal cation complexes, resulting in a much stronger interaction between the ferrocenyl group and the macrocycle-bound cation as revealed by our voltammetric results.

The cyclic voltammetry of compound **2** is also strongly affected by additions of substoichiometric concentrations of Ag^+ ion. Qualitatively, the changes are similar to those observed in the presence of Na^+ ion (see Figure 12A). This finding is extremely interesting since, to the best of our knowledge, this is the *first reported example of redox-switching of Ag^+ complexation.* Surprisingly, the $\Delta E_{1/2}$ value is much larger than that observed with Na^+ ion. In fact, it is even slightly larger than the value observed with Ca^{2+} (see Table V). This is inconsistent with the relatively small charge-to-size ratio of the Ag^+ cation. Thus, the Ag^+ data point falls clearly off the straight line of the plot in Figure 10. The fact that Ag^+ ion exerts a much larger effect on the half-wave potential of the ferrocenyl group than would be predicted in terms of its charge-to-size ratio suggests that the bound Ag^+ cation resides closer to the ferrocenyl subunit than any of the other alkali and alkaline-earth cations surveyed in this work. This is indeed in perfect agreement with the X-ray crystallographic, UV, and NMR data (vide supra) of this complex and indicates that the ferrocenyl group acts as a donor toward the d-orbital-bearing Ag^+ cation.

b. Cyclic Voltammetry of 1, 4, 6, 8, and 9 in the Presence of Metal Cations. Compound **1** exhibits a half-wave potential of 0.622 V versus SSCE for the reversible oxidation of the ferrocenyl group. Hall and co-workers have reported that **1** does not exhibit

changes in its voltammetric behavior upon addition of Na^+ and K^+ ions.[12f] Our observations agree with their report. In addition, we do not observe any voltammetric changes upon addition of Ag^+ ion. This further verifies that the amide linkages between the ferrocenyl and macrocyclic subunits seriously diminish the binding ability of this class of redox-active macrocycles.

Ligand **4** shows a single set of waves centered at 0.395 V versus SSCE which corresponds to the almost simultaneous, but independent, oxidation of the two ferrocenyl moieties. Resolved, two-wave voltammetric behavior in the presence of substoichiometric concentrations of either Ag^+ or Na^+ ions is not observed. However, the presence of either ion shifts the half-wave potential to more positive values. Addition of 1 equiv of Na^+ shifts the potential to a value of 0.428 V. The corresponding value for 1 equiv of Ag^+ is 0.500 V. This reveals weaker binding between the neutral form of **4** and these cations rendering **4** a relatively inefficient redox-active ligand. Ligand **6**, however, shows more interesting properties associated with its dimeric structure that contains two ferrocenyl subunits and two diaza-18-crown-6 macrocyclic rings. In the absence of small cations, **6** shows a single redox couple (0.382 V) that corresponds to the simultaneous oxidation of both ferrocenyl subunits. In the presence of 1 equiv of Ag^+ ion, a new redox couple at 0.575 V is observed (see Figure 12B). The peak currents for this redox couple increase with $[Ag^+]$ until they reach full development when the Ag^+ concentration is exactly twice that of ligand **6**. If this level of Ag^+ concentration is exceeded, metallic Ag deposits at the working electrode surface since the initial potential is sufficiently negative to reduce Ag^+ to the metallic form. The presence of Ag deposits can be ascertained from the sharp anodic peak observed on the anodic scan at 0.24 V which corresponds to the anodic stripping of the metallic silver. This peak is not observed if the Ag^+ concentration is kept below the level of 2 equiv since complexation by **6** keeps the concentration of free Ag^+ ion very low, preventing its reduction at the electrode surface. This result is in accord with the FAB/MS results noted above.

All these observations suggest that derivative **6** is also an effective redox-switchable ligand for Ag^+. In addition, two Ag^+ ions can be complexed by one molecule of **6**. The strong effect of Ag^+ ions on the voltammetric behavior of **6** suggests that the binding sites for the two Ag^+ cations are located inside the cavity formed by the two macrocyclic rings and the two ferrocenyl subunits. Na^+, K^+, and Ca^{2+} ions also affect the electrochemistry of **6** but less markedly than Ag^+ ion. Addition of perchlorate salts of either one of these cations shifts, to various extents, the half-wave potential for reversible oxidation of the dimeric ligand. At the level of two cation equivalents the apparent half-wave potentials are: 0.470 V (Na^+), 0.450 V (K^+), and 0.520 V (Ca^{2+}). At ion concentrations below the level of 2 equiv, the voltammetric peaks are broad, perhaps hinting unresolved splitting of waves corresponding to the free and bound forms of the ligand.

Compound **9** was prepared to investigate the effectiveness of two aminic nitrogens and the ferrocenyl group as a set of donors for Ag^+ ion. This compound does not contain a macrocyclic ring. Cyclic voltammetry of **9** in CH_3CN/0.1 M $TBA^+PF_6^-$ shows the expected reversible oxidation at 0.397 V attributable to the ferrocene group. The voltammetric features do not change upon the addition of up to 3 equiv of Ag^+ ion, indicating that **9** is a much weaker ligand for this ion than **2** or **6**. Therefore, the presence of two freely rotating aminic nitrogen atoms attached to a ferrocenyl subunit does not by itself constitute a very efficient binding structure for Ag^+, although the arrangement seems to be quite effective when inserted into an appropriate macrocyclic framework.

Finally, the reversible oxidation of derivative **8** was observed at a half-wave potential of 0.755 V. Additions of Na^+ ion did not cause any shifts in this potential value. Thus, this derivative seems to be a particularly poor ligand that does not show any redox-switching ability.

c. Aqueous Electrochemistry of 2 in the Presence of Silver Ions. The strong interaction of **2** with Ag^+ in acetonitrile led us to try similar voltammetric experiments in aqueous solution in the hope that the **2**·Ag^+ complex would be stable enough in this medium

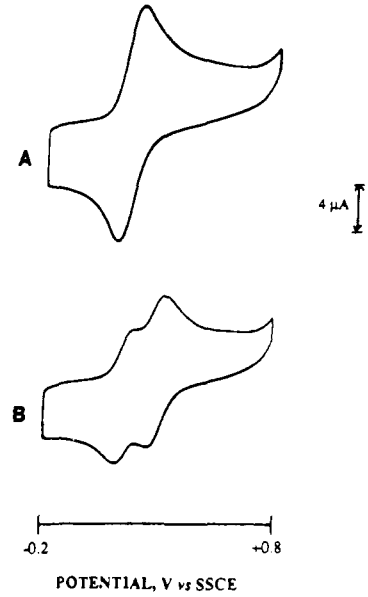

Figure 13. Voltammetric response of **2** in aqueous media containing 0.1 M KNO_3 as supporting electrolyte, scan rate = 100 mV/s: (A) 0.7 mM ligand **2**. (B) 0.7 mM ligand **2** + 0.35 mM Ag^+.

to allow the observation of substantial changes in the electrochemistry of this ligand. As expected, the reversible oxidation of **2** in aqueous medium is not affected by the addition of alkali metal or calcium salts to the solution (see Figure 13A). Thus, we used KNO_3 as the supporting electrolyte. Protonation of the tertiary nitrogens of **2** does affect the voltammetric behavior since the protonated forms undergo reversible oxidation at more positive potentials. However, addition of 0.5 equiv of $AgNO_3$ to the medium results in the observation of a new redox couple whose peak currents increase with the concentration of Ag^+ ion (Figure 13B). Upon the addition of 1.0 equiv of Ag^+, the original redox couple disappears and the new couple reaches full development. This behavior is qualitatively similar to that observed in acetonitrile and reveals that the binding constant for the **2**·Ag^+ complex is also substantially high in water. Furthermore, the observation of two-wave behavior with substoichiometric concentrations of Ag^+ indicates that ligand **2** acts as an effective redox-switchable ligand for Ag^+ ion in aqueous medium. To the best of our knowledge, this is the *first reported example of redox switching ability by a ligand in aqueous medium.* From digital simulations we estimate the minimum values of the Ag^+ binding constants with **2** as $K = 7 \times 10^5$ and $K_+ = 1 \times 10^3$ M^{-1}.

The Nature of Silver Complexation by 2. This work demonstrated that compound **2** is an efficient ligand for alkali metal, calcium, and silver ions. In these complexes the cation is encapsulated inside **2** which acts as a ligand of the cryptand class, providing a well-defined cavity for the metal ion. While the interactions of Na^+, K^+, and Ca^{2+} with the macrocycle are essentially of the ion–dipole type, this does not seem to be the case with Ag^+. First, the X-ray crystal structure of the **2**·Ag^+ complex exhibits a much shorter Ag–Fe distance than the corresponding Na–Fe distance in the **2**·Na^+ complex. Second, the difference between the formal potentials of the oxidation of the cation complex and the free ligand correlates linearly with the charge-to-size ratio of the metal cation for Na^+, K^+, and Ca^{2+}. Interestingly, Ag^+ has a much larger effect than expected from its relatively small charge-to-size ratio. Third, complexation of **2** by alkali or alkaline-earth metal ions has a small effect on its electronic absorption spectrum. Once again, Ag^+ is unusual in that the absorption peak at λ_{max} = 440 nm, characteristic of the ferrocene group, is shifted by 20 nm.

All these data indicate that in the metal ion complexes of **2** the silver cation resides closer to the ferrocene group than the other cations. Therefore, the silver ion exerts the greatest effect on the electrochemical and spectral properties of the ferrocene group. The reasons for the closer approach of Ag^+ to the ferrocene subunit

are probably related to orbital interactions between the two entities. Ag^+ is the only one among the surveyed ions that has readily available d orbitals. In fact, there are literature precedents for M^+–Fe bonds in several kinetically inert complexes of transition metal ions in which a ferrocenyl group acts as a donor in the coordination sphere of the metal ion.[13,25] Our data clearly suggest that similar interactions take place in the **2**·Ag^+ complex. However, this complex has a dynamic nature (it is kinetically labile). Thus, **2** is the first example of a dynamic ligand in which the ferrocenyl group acts as a donor group. The combination of the Ag^+–ferrocene interaction and the presence of two axial atoms explains the Ag^+ selectivity exhibited by compound **2** and their dimeric analogues **4** and **6**.

Conclusions

Reduction of the amide residues of **1** affords a ligand (**2**) that behaves as a cryptand rather than simply interacting superficially with cations as has been the case with **1** and other related systems. The cryptand cation inclusion structure was confirmed for Na^+ and Ag^+ by solid-state (X-ray) analysis. The Na^+ complexation behavior of **2** is typical of a cryptand as shown by ^{23}Na NMR. Electrochemical studies confirm the strength of binding with a variety of cations and also the ability to undergo redox switching. Among the cations studied, the first example of such behavior with Ag^+ cation was observed. Indeed, voltammetric evidence for redox-switching behavior in water was obtained with Ag^+. The special strength of the **2**·Ag^+ interaction is attributed to the d-electrons present in ferrocene. This interaction, unprecedented in kinetically labile systems, was confirmed by UV–visible spectroscopy and suggests that the ferrocene group may be far more versatile in such applications than originally thought.

Experimental Section

General Information. ^1H NMR spectra were recorded on a Varian XR-400 high resolution NMR spectrometer or on a Hitachi Perkin-Elmer R-600 NMR spectrometer in $CDCl_3$ solvents and are reported in ppm (δ) downfield from internal $(CH_3)_4Si$. ^{13}C NMR were recorded on a JEOL FX90Q or Varian XL-400 NMR spectrometer or as noted above. Infrared spectra were recorded on a Perkin-Elmer 1310 infrared spectrophotometer and were calibrated against the 1601-cm^{-1} band of polystyrene. Melting points were determined on a Thomas Hoover apparatus in open capillaries and are uncorrected. Thin layer chromatographic (TLC) analyses were performed on aluminum oxide 60 F-254 neutral (Type E) with a 0.2-mm layer thickness. Preparative chromatography columns were packed with activated aluminum oxide (MCB 80-325 mesh, chromatographic grade, AX 611).

Methanol employed in the stability constant determination was purchased from Mallinkrodt, anhydrous grade, and was further dried by distillation over magnesium turnings. The acetonitrile employed in the stability constant determinations was ACS reagent grade purchased from Aldrich Chemical Co. and was dried over 4-Å molecular sieves. Electrochemical, puriss. grade, tetrabutylammonium hexafluorophosphate was obtained from Fluka and was used without further purification. When tetrabutylammonium hexafluorophosphate from Aldrich Chemical Co. with purity ≈98% was used, the material was recrystallized from methanol, and dried in a vacuum oven (60 °C, 0.05 mmHg) for 48 h prior to use. $NaClO_4$, KCl, and $KClO_4$ were of the highest purity sold by Aldrich, and they were recrystallized from H_2O and dried in a vacuum oven as above for 48 h prior to use. The $AgNO_3$ used was purchased from Aldrich Chemical Co. ("Gold Label," specified purity of 99.9999%) and was used without further purification. $Ca(ClO_4)_2$ was purchased from Alfa and was vacuum dried as above prior to use. Other materials used were purified by standard methods.

All reactions were conducted under dry N_2 unless otherwise noted. All reagents were the best grade commercially available and were distilled, recrystallized, or used without further purification, as appropriate. Combustion analyses were performed by Atlantic Microlab, Inc., Atlanta, GA, and are reported as percents.

Stability Constants. Unless otherwise specified, cation binding constants were measured in absolute MeOH at 25.0 ± 1.0 °C using a Corning 476210 electrode and an Orion Model 701A "ionalyzer" meter according to the method of Frensdorff[17a] as described recently in detail.[17b] Values for the equilibrium constants are reported as log K_S. The stability constants in methanol and acetonitrile were obtained with the help of an Orion Model 701A ion/pH meter. Sodium activities in methanol were determined using a Corning ISE Model 476210, Potassium activities were recorded with the help of Corning monovalent cation electrode, Model 476220; in both cases a Ag/AgCl reference electrode from Corning (Model 476029) was employed. Temperature during the stability constants determination was kept constant at 25.0 ± 0.1 °C with the help of Cole-Palmer Model 1253-00 water circulator. The solutions were constantly stirred, except during readings; the temperature inside the cell was check with the help of a Cole-Palmer thermocouple, Model 8508-45, fitted with an extension cable. The procedure followed has previously been described.[17b] The method was calibrated using 18-crown-6 and both Na^+ and K^+. The expected binding constants (log K_S 4.38 and 6.02, respectively) validated the method.[17b] The determination of the stability constant of **1** with Ag^+ in acetonitrile was obtained by potentiometric titration with a solution of the cryptand **1**. The ionic strength of the solutions was kept constant at 0.1 M in tetrabutylammonium hexafluorophosphate, the concentration of supporting electrolyte used in the cyclic voltammogram experiments. The stability constants for the other cations in acetonitrile were determined by competition experiments against Ag^+ cation. Additional details are available.[18] Control experiments using 4,7,13,16,21,24-hexaoxa-1,10-diazabicyclo[8.8.8]hexacosane ([2.2.2]cryptand) as the host with Ag^+ and Na^+ (log K_S = 8.96 and 9.8, respectively) validated the method.[19,26]

Electrochemistry. Acetonitrile was HPLC quality from EM Science. Tetrabutylammonium hexafluorophosphate was purchased from Fluka and used without further purification. All other salts were of the best quality commercially available.

a. Equipment. The electrochemical experiments were performed with a Princeton Applied Research Model 173/175/179 setup, and the current–potential traces were recorded on a Soltec VP-6423S X–Y recorder. The rotating disk electrode voltammograms were obtained using a Pine Model ASR analytical rotator assembly.

b. Electrochemical Experiments. Cyclic voltammetric data were recorded using a glassy carbon working electrode (0.082 cm^2), a platinum counterelectrode, and a sodium saturated calomel half-cell as the reference electrode. Glassy carbon electrode surfaces were polished with 0.05-μm alumina, sonicated in water, and air-dried immediately before use. The acetonitrile solution (containing 0.1 M $TBA^+PF_6^-$, as supporting electrolyte, 0.5–1.0 mM of the ligand, and variable concentrations of metal salts) was placed in a single-compartment electrochemical cell and degassed by bubbling with N_2(g) saturated with acetonitrile. A N_2 atmosphere was continuously maintained above the solution while the experiments were in progress.

c. Digital Simulations. Digital simulations used in this work are based on previous work by our groups in which we successfully simulated the behavior of other redox-switchable ligands. Assumptions made for these simulations are: (a) one electron is reversibly transferred in the electrochemical process; (b) the chemical and electrochemical equilibria are fast on the experimental time scale; (c) the diffusion coefficients are the same for all species; and (d) the electrode is planar.

Each simulation required the following parameters: the initial and switching potentials, the scan rate, the ligand and metal cation concentrations, the half-wave potential for the free ligand, the binding constant of the ligand with the metal cation, and the binding constant of the oxidized form of the ligand with the metal cation. A scan step size of 2 mV was utilized in the calculations. Each iteration of the simulation goes through the following steps: (i) establishment of the initial conditions based on the potential and binding constants; (ii) diffusion of all species through a 4.2 $N^{1/2}$ diffusion layer, where N is the number of iterations already calculated; (iii) reestablishment of equilibria at the electrode surface; (iv) calculation of the current flow from the flux of electroactive material at the electrode surface.

The simulation program was written in Fortran 77 and compiled with the Microsoft Fortran Compiler (Version 4.0). Simulations were run on several IBM compatible microcomputers equipped with floating point coprocessors. The simulation program source code is available upon request (to A.K.).

Fast Atom Bombardment Mass Spectrometry. Fast atom bombardment spectra were acquired on a VG Trio 2 quadrupole mass spectrometer equipped with the Lab-Base data system. An 8-kV xenon atom beam was used to desorb samples from the 3-nitrobenzyl alcohol FAB matrix. In a typical experiment, 1 μL of matrix, 1 μL of a 12 mM macrocycle solution (CH_3CN), and 1 μL of a 12 mM cation (as the

(25) (a) Akabori, S.; Kumagai, T.; Shirahige, T.; Sato, S.; Kawazoe, K.; Tamura, C.; Sato, M. *Organometallics* **1987**, *6*, 2105. (b) Sato, M.; Sekino, M.; Akabori, S. *J. Organomet. Chem.* **1988**, *344*, C31. (c) Sato, M.; Asano, H.; Suzuki, K.; Katada, M.; Akabori, S. *Bull. Chem. Soc. Jpn.* **1989**, *62*, 3828.

(26) (a) Cox, B. G.; Guminski, C.; Schneider, H. *J. Am. Chem. Soc.* **1982**, *104*, 3789. (b) Cox, B. G.; Garcia-Rosas, J.; Schneider, H. *J. Am. Chem. Soc.* **1981**, *103*, 1384. (c) Buschmann, H.-J. *Inorg. Chim. Acta* **1986**, *120*, 125.

perchlorate) solution (CH_3CN) were carefully mixed on the FAB probe. Typically 10 scans were combined to produce the spectra used for intensity ratios. Binding trends were assessed from the ratio of [macrocycle·cation] complex to protonated macrocycle. The data for sodium binding resulted from single determinations; however, the silver data resulted from the average of a minimum of three separate assays.

Ferrocene Starting Materials. 1,1′-Ferrocenedicarboxylic acid was purchased from Aldrich Chemical Co. and used without further purification. Preparation of 1,1′-bis(chlorocarbonyl)ferrocene was accomplished by treatment of 1,1′-ferrocenedicarboxylic acid with oxalyl chloride followed by a catalytic amount of pyridine as reported by Petrovitch.[27]

1,1′-(1,4,10,13-Tetraoxa-7,16-diazacyclooctadecane-7,16-diyldicarbonyl)ferrocene (1) and 1,1″:1′,1‴-Bis(1,4,10,13-tetraoxa-7,16-diazacyclooctadecane-7,16-diyldicarbonyl)bisferrocene (5). 1,1′-(1,4,10,13-Tetraoxa-7,16-diazacyclooctadecane-7,16-diyldicarbonyl)-ferrocene, and 1,1″:1′,1‴-bis(1,4,10,13-tetraoxa-7,16-diazacyclooctadecane-7,16-diyldicarbonyl)bisferrocene was prepared simultaneously according to the literature procedure[4] by reaction of equimolar amounts of 1,1′-ferrocenedicarboxylic acid chloride and 4,13-diaza-18-crown-6 in the presence of Et_3N with benzene as the solvent under high dilution conditions (7 mM). After purification by chromatography in alumina 1,1′-(1,4,10,13-tetraoxa-7,16-diazacyclooctadecane-7,16-diyldicarbonyl)ferrocene and 1,1″:1′,1‴-bis(1,4,10,13-tetraoxa-7,16-diazacyclooctadecane-7,16-diyldicarbonyl)bisferrocene were obtained in 48 and 8% yield, respectively.

1,1′-(1,4,10,13-Tetraoxa-7,16-diazacyclooctadecane-7,16-diyldimethyl)ferrocene (2). Reduction was effected by stirring a mixture of **1** (2.0 g, 4 mmol) at ambient temperature under N_2 in 100 mL of a 15% by volume solution of THF in CH_2Cl_2 with $LiAlH_4$ (600 mg, 16 mmol). The reaction mixture was stirred for 30 min, then diluted with CH_2Cl_2 (50 mL), and quenched with a saturated aqueous solution of Na^+K^+ tartrate (75 mL). The organic layer was separated and washed with (deionized) water (3 × 75 mL). The organic layer was then dried over $MgSO_4$, the solvent was evaporated in vacuo, and the residue was chromatographed over alumina (deactivated with 3% H_2O) and eluted with 1% CH_3OH/CH_2Cl_2 v/v. The product was collected and recrystallized from a $(CH_3CH_2)_2O$/hexane mixture (99:1 v/v) to afford **2**·H_2O (1.2 g, 61%) as yellow-orange crystals, mp 101–104 °C. ^1H NMR: 2.66 (m, 4 H), 2.80 (m, 4 H), 3.67 (m, 16 H), 3.80 (m, 4 H), 4.05 (s, 4 H), 4.26 (s, 4 H). ^{13}C NMR ($CDCl_3$) 53.364, 54.056, 67.014, 69.680, 70.583, 87.103. Mass spectrum [DCI, m/z (relative intensity)]: 132 (20), 214 (10), 263 (60), 472 (<1, M^+), 473 (1, $M + H^+$), 474 (<1, $M + 2H^+$. IR (KBr): 3400 (s), 2820 (s), 1435 (m), 1270 (s), 1100 (s), and 800 (m) cm^{-1}. Anal. Calcd for $C_{24}H_{36}N_2O_4Fe·H_2O$: C, 58.79; H, 7.81. Found: C, 58.79; H, 7.80.

(1,4,10,13-Tetraoxa-7,16-diazacyclooctadecane-7,16-diyldicarbonyl)-bisferrocene (3). (1,4,10,13-Tetraoxa-7,16-diazacyclooctadecane-7,16-diyldicarbonyl)bisferrocene was prepared in 84% yield by reacting ferrocenecarboxylic acid chloride in benzene with a solution of diaza-18-crown-6 and Et_3N according to the literature.[5]

(1,4,10,13-Tetraoxa-7,16-diazacyclooctadecane-7,16-diyldimethyl)-bisferrocene (4). (1,4,10,13-Tetraoxa-7,16-diazacyclooctadecane-7,16-diyldicarbonyl)bisferrocene (686 mg, 1 mmol) was dissolved in 10 mL of a CH_2Cl_2 and THF mixture (2:1 v/v). Then to it was added in portions $LiAlH_4$ (114 mg, 3 mmol). The reaction mixture was then stirred for 18 h and the excess $LiAlH_4$ quenched with water (25 mL). The mixture was extracted three times with CH_2Cl_2 (75 mL) and dried over $MgSO_4$, the product was chromatographed in alumina with 1% $MeOH/CH_2Cl_2$ (v/v) to afford the product as a yellow solid (480 mg, 88% yield), mp 114–116 °C. ^1H NMR: 2.71 (t, J = 5 Hz, 8 H), 3.56 (m, 20 H), 4.09 (bs, 14 H), 4.14 ppm (s, 4 H). IR (KBr): 3100 (m), 2895 (s), 1360 (m), 1300 cm^{-1} (m). DCI (CH_4): m/z (relative intensity) 658 (4, M^+), 459 (2), 199 (100). Anal. Calcd for $C_{34}H_{46}N_2O_2Fe_2$: C, 62.02; H, 7.04. Found: C, 61.90; H, 7.02.

1,1″:1′,1‴-Bis(1,4,10,13-tetraoxa-7,16-diazacyclooctadecane-7,16-diyldimethyl)bisferrocene (6). 1,1″:1′,1‴-Bis(1,4,10,13-tetraoxa-7,16-diazacyclooctadecane-7,16-diyldicarbonyl)bisferrocene (2.1 g, 2.1 mmol) was dissolved in a mixture of CH_2Cl_2 (20 mL) and THF (20 mL) and to it was added in portions $LiAlH_4$ (2 g, 53 mmol). The reaction mixture was allowed to stir for 6 h before quenching by dropwise addition of H_2O. After the excess $LiAlH_4$ was consumed, the mixture was dissolved with 200 mL CH_2Cl_2 and washed (3×) with an equal volume of H_2O. The organic layer was dried over $MgSO_4$, the solvent evaporated, and the residue chromatographed over alumina with 1% $MeOH/CH_2Cl_2$ (v/v); the product was further purified by recrystallization from an Et_2O/CH_2Cl_2 mixture to afford 1.2 g of product as yellow needles (1.2 g, 64% yield), mp 104–105 °C. ^1H NMR: 2.73 (t, J = 5 Hz, 16 H), 3.58–3.69 (m, 40 H), 4.07 (t, J = 2 Hz, 8 H), 4.10 ppm (t, J = 2 Hz, 8 H). ^{13}C NMR: 53.313, 54.080, 68.409, 69.524, 70.715, 70.761, 83.558 ppm. IR (KBr): 3380 (s), 2850 (s), 1440 (w), 1350 (m), 1105 cm^{-1} (s). FAB (*m*-nitrobenzyl alcohol): m/z (relative intensity) 945 (1, M^+), 473 (100). Anal. Calcd for $C_{48}H_{72}N_4O_8Fe_2$: C, 61.02; H, 7.68; N, 5.93. Found: C, 60.78; H, 7.69; N, 5.95.

Ferrocenylmethyl 3-Cholestanyl Ether (7). Ferrocenylmethyl 3-cholestanyl ether was prepared according to the procedure previously published by us.[7] To dimethylaminomethylferrocene (749 mg, 3 mmol) in acetone (30 mL) was added dihydrocholesterol (1.16 g, mmol) followed by addition of methyl iodide (426 mg, 3 mmol); the reaction was then set to reflux for 72 h. Afterwards, the solvent was evaporated and the crude diluted with H_2O and extracted 3× with CH_2Cl_2; the organic layers were combined and dried with brine and $MgSO_4$. The solvent was evaporated and chromatographed over silica using 1:20 EtOAc/hexane (v/v). The product was recrystallized from acetone to afford the product as a yellow solid (119 mg, 7% yield), mp 134–136 °C, $[\alpha]_D$ = +11.8 (c = 1, CH_2Cl_2). ^1H NMR: 0.64 (s), 0.77 (s), 0.86 (d, J = 5.4 Hz), 0.89 (d, J = 6.4 Hz), 0.45–2.2 (steroidal, 46 H), 3.28 (m, 1 H), 4.14 (s, 7 H), 4.25 (s, 2 H), 4.27 ppm (s, 2 H). ^{13}C NMR: 84.499, 77.641, 77.216, 69.327, 69.327, 68.409, 68.409, 68.409, 68.409, 68.409, 68.295, 68.295, 65.982, 56.560, 56.340, 54.482, 44.969, 42.633, 40.099, 39.537, 37.095, 36.200, 35.805, 35.540, 34.910, 32.179, 28.925, 28.356, 28.265, 28.022, 24.237, 23.850, 22.818, 22.568, 21.256, 18.692, 12.312, 12.092 ppm. IR (KBr): 2950 (d), 2900 (d), 1460 (d), 1100 cm^{-1} (m). DCI (CH_4): m/z (relative intensity) 587 (<1, $M + H^+$), 586 (<1, M^+), 371 (8), 19 (100). Anal. Calcd for $C_{38}H_{58}FeO$: C, 77.79; H, 9.96. Found: C, 77.89; H, 10.02.

1,1″-(1,4,10,13-Tetraoxa-7,16-diazacyclooctadecane-7,16-diyldicarbonyl)-1′,1‴-bis(carbomethoxy)bisferrocene (8). 1,1″-(1,4,10,13-Tetraoxa-7,16-diazacyclooctadecane-7,16-diyldicarbonyl)-1′,1‴-bis(carbomethoxy)bisferrocene was prepared according to the procedure previously published by us. 4,13-Diaza-18-crown-6 (375 mg, 1.4 mmol) and Et_3N (1 mL, 7 mmol) are dissolved in benzene (15 mL); over a period of 20 min a solution of 1-(chlorocarbonyl)-1′-(carbomethoxy)ferrocene[28] (878 mg, 2.9 mmol) in benzene (10 mL) was added dropwise. The reaction mixture was allowed to stir for 3 h; then the solvent was evaporated and the residue chromatographed over silica using 1:99 $MeOH/CH_2Cl_2$, affording the product as a yellow powder (511 mg, 44% yield), mp 141–143 °C. ^1H NMR: 3.64 (s, 8 H), 3.72 (bs, 16 H), 3.80 (s, 6 H), 4.32 (s, 4 H), 4.46 (s, 4 H), 4.64 (s, 4 H), 4.84 ppm (s, 4 H). IR (KBr): 3100 (w), 2980–2890 (w), 1715 (s), 1610 cm^{-1} (s). DCI (CH_4): m/z (relative intensity) 803 (3, M + 1), 679 (1), 271 (10), 125 (100), 92 (45). Anal. Calcd for $C_{38}H_{46}N_2O_{10}Fe_2$: C, 56.88; H, 5.78. Found: C, 56.88; H, 5.82.

1,1′-Bis(dimethylaminomethyl)ferrocene (9). Previously known[6] bis(dimethylaminomethyl)ferrocene was prepared by reduction of bis(dimethylaminocarbonyl)ferrocene[12f] (2.5 g, 8.3 mmol) in THF (50 mL) with $LiAlH_4$ (1.0 g, 26 mmol). The reaction was quenched by dropwise addition of water to consume the excess hydride. The mixture was then diluted with CH_2Cl_2 (75 mL) and washed with an equal volume of water. The organic phase was evaporated and the oily residue chromatographed over alumina to afford **9** (300 mg, 12%) as an amber oil whose spectral properties matched literature values.[6]

***N,N′*-Bis(benzyl)-4,13-diaza-18-crown-6 (10)** was purchased from Aldrich Chemical Co. and recrystallized from ethanol prior to use.

X-ray Structure Determinations. a. Cryptand 2-Hydrate. Crystals of **2**·H_2O suitable for X-ray analysis were obtained by slow evaporation of a 1% (v/v) hexane–ether solution to afford yellow-orange crystals. The structure determination was performed on an Enraf-Nonius CAD-4F diffractometer using a graphite monochromater, capillary mounted, radiation Mo-Kα. The plate-shaped, monoclinic crystal was approximately 0.11 × 0.62 × 0.93 mm, space group $P2_1/n_1$, a = 9.932(2), b = 11.195(1), c = 22.249(4) Å; V = 2429 Å^3, β = 100.97(2)°, λ (Mo-Kα) = 0.71069 Å, Z = 4, D_c = 1346 g·cm^{-3}, total number of reflections and unique reflections 4853 and 4579, respectively, R = 0.037, R_w = 0.041. All nonhydrogen atoms were refined with anisotropic thermal parameters. The hydrogen atoms bonded to **1** were placed in calculated positions and allowed to ride on the bonded carbon atoms. The two hydrogen atoms of the water molecule were located on a difference Fourier map and were not refined. Atomic coordinates, bond lengths and angles, and thermal parameters have been deposited at the Cambridge Crystallographic Data Centre.

b. Cryptand 2·Na^+. The $NaClO_4$ complex of **2** was obtained by dissolving 1 equiv of **2** in a solution containing 1.5 equiv of the salt in Me_2CO. The solvent was evaporated under reduced pressure and the

(27) Petrovitch, P. *Double Liaison* **1966**, *133*, 1093; *Chem. Abstr.* **1968**, *68*, 29843g.

(28) Yamakawa, K.; Ouchi, H.; Arakawa, K. *Chem. Pharm. Bull.* **1963**, 11 905; *Chem. Abstr.* **1963**, 59; 8787b.

remaining crystals were suspended in $CHCl_3$. The solution was filtered, the volume of $CHCl_3$ was reduced under a stream of Ar, and the crystals were allowed to form under vapor diffusion conditions in the freezer using Et_2O as the equilibrating solvent. The vapor diffusion recrystallization was repeated to afford the complex as orange-red crystals, mp 208–215 °C. Anal. Calcd for $C_{24}H_{36}ClFeN_2NaO_8$: C, 48.46; H, 6.10; N, 4.71. Found: C, 48.42; H, 6.09; N, 4.68. The thin, needle-shaped crystals were mounted in thin-walled glass capillaries prior to X-ray diffraction analysis. The crystal belongs to the *Pbcn* space group, with maximum dimensions of 0.10 × 0.10 × 0.20 mm, the cell dimensions were a = 10.833 (Å), b = 17.167(3) Å, c = 14.718(2) Å, V = 2737 Å^3, D_c = 1.45 g/cm^3, ν_c = 1.8 cm^{-1}, molecules/unit cell = 4, λ = MoKα; total number of reflections collected and observed were 2621 and 962, respectively, R = 0.052, R_w = 0.052. All nonhydrogen atoms were treated with anisotropic thermal parameters. The hydrogen atoms were placed in geometry-fixed positions and were not refined. The weighting scheme was based upon unit weights. A final difference electron density map displayed no unaccounted electron density.

c. **Cryptand 2·Ag$^+$.** The $AgClO_4$ complex of **2** was prepared by simultaneously mixing acetone solutions containing equivalent amounts of **2** and salt. The solvent was evaporated under reduced pressure; the residue was dissolved in $CHCl_3$ and then filtered. The solvent was reduced (Ar stream) to 0.5 mL. Two vapor diffusion crystallizations (0.5 mL of $CHCl_3$/4 mL of Et_2O) afforded the complex as orange plates (mp 209–210 °C). Small, thin plates of the compound were mounted in thin-walled glass capillaries prior to X-ray diffraction analysis. Details of the procedure have been given previously.[29] The maximum crystal dimensions were 0.05 × 0.10 × 2.0 mm. The space group is $P2_1/n$, the cell constants were a = 17.186(2) Å, b = 9.152(1) Å, c = 17.802(1) Å, β = 108.93(1)°, V = 2649 Å^3, molecules/unit cell = 4, D_c = 1.71 g/cm^3, μ = 1.5 cm^{-1}, λ = MoKα, reflections collected = 5121, reflections observed = 1900, R = 0.056, R_w = 0.061. The structure was solved using SHELX-86. All nonhydrogen atoms were treated with anisotropic thermal parameters. The hydrogen atoms were placed in geometry-fixed positions and were not refined. A final difference electron density map displayed no unaccounted electron density.

Acknowledgment. We thank the National Institute of Health (to G.W.G., GM 36262) and the National Science Foundation (to A.K. CHE 9000531) for grants that supported this work.

Supplementary Material Available: FAB/MS spectra of **1**·Ag$^+$, **2**·Ag$^+$, and **6**·Ag$^+$ and figure of equilibrium concentration of the **2**·Na$^+$ complex as the potential is scanned across the $E^{\circ\prime}$ value of the **2**$^+$/**2** couple (5 pages). Ordering information is given on any current masthead page.

(29) Holton, J.; Lappert, M. F.; Ballard, D. G. H.; Pearce, R.; Atwood, J. L.; Hunter, W. E. *J. Chem. Soc., Dalton Trans.* **1979**, 45.

Dissociative Electron Transfer. New Tests of the Theory in the Electrochemical and Homogeneous Reduction of Alkyl Halides

Jean-Michel Savéant

Contribution from the Laboratoire d'Electrochimie Moléculaire de l'Université de Paris 7, Unité Associée au CNRS No. 438, 2 place Jussieu, 75251 Paris Cedex 05, France.
Received May 26, 1992

Abstract: In the testing of the theory of dissociative electron transfer with experimental data pertaining to the electrochemical and homogeneous reduction of alkyl halides, uncertainties arising from the estimation of the effect of solvent dynamics and reorganisation as well as of the resonance energy in the transition state are minimized by a comparative strategy which utilizes information derived from outer-sphere electron-transfer data gathered in the same solvent. Application of this strategy leads to a good agreement between theory and experiment in the electrochemical case. In the homogeneous case, the agreement is equally satisfactory in the case of tertiary halides. With the less sterically hindered secondary and primary halides, the reaction possesses an S_N2 character involving small bonded interactions in the transition state in accord with previous stereochemical results and reaction entropy determinations.

As shown earlier,[1] important assumptions underlying the Marcus–Hush model[2] of outer-sphere electron-transfer dynamics are not applicable to dissociative electron transfer. In the latter type of reaction, electron transfer from an electrode or from an outer-sphere homogeneous electron donor, D$^{\bullet-}$, to the acceptor molecule, RX, is concerted with the breaking of the R–X bond:

$$\text{electrochemical: } RX + e^- \rightleftarrows R^\bullet + X^-$$

$$\text{homogeneous: } RX + D^{\bullet-} \rightleftarrows R^\bullet + X^- + D$$

Representation of the potential energy by the R–X Morse curve in the reactant system and by a purely dissociative curve identical to the repulsive part of the R–X curve in the R$^\bullet$ + X$^-$ system and treatment of solvent reorganization in the Marcus–Hush fashion lead to a quadratic activation–driving force relationship:[1]

$$\Delta G^\ddagger = w_R + \Delta G_0^\ddagger\left(1 + \frac{\Delta G^\circ - w_R + w_P}{4\Delta G_0^\ddagger}\right)^2 \qquad (1)$$

(ΔG° is the standard free energy of the reaction, i.e., the opposite of the driving force in terms of free energy; $\Delta G_0^\ddagger$ is the standard activation free energy, i.e., the activation free energy of the forward and reverse reactions at zero driving force or, in other words, the intrinsic barrier free energy; w_R is the work required for bringing the reactants from infinity to reacting distance, i.e., to form the "precursor complex"; w_P is the work required to form the "successor complex", from infinity to reacting distance) where the intrinsic barrier $\Delta G_0^\ddagger$ is, neglecting the possible internal changes besides bond breaking (or assuming they are included in the Morse curve description), the sum of two terms:

(1) (a) Savéant, J.-M. *J. Am. Chem. Soc.* **1987**, *109*, 6788. (b) Savéant, J.-M. *Adv. Phys. Org. Chem.* **1990**, *26*, 1.

(2) (a) Marcus, R. A. *J. Chem. Phys.* **1956**, *24*, 4966. (b) Hush, N. S. *J. Chem. Phys.* **1958**, *28*, 962. (c) Marcus, R. A. Theory and Applications of Electron Transfers at Electrodes and in Solution. *Special Topics in Electrochemistry*; Rock, P. A., Ed.; Elsevier: New York, 1977; pp 161–179. (d) Marcus, R. A. *Faraday Discuss. Chem. Soc.* **1982**, *74*, 7. (e) Marcus, R. A.; Sutin, N. *Biophys. Biochim. Acta* **1985**, *811*, 265.

0002-7863/92/1514-10595$03.00/0